Plasmon-induced excitation energy transfer in silver nanoparticle dimers: a real-time TDDFTB investigation

Cite as: J. Chem. Phys. (in press) (2021); https://doi.org/10.1063/5.0082960
Submitted: 20 December 2021 • Accepted: 27 March 2022 • Accepted Manuscript Online: 28 March 2022

Zhen Liu, Maria Belen Oviedo, Bryan Matthew Wong, et al.

Accepted to J. Chem. Phys. 10.1063/5.0082960

Plasmon-induced excitation energy transfer in silver nanoparticle dimers: a real-time TDDFTB investigation

Zhen Liu,[a] *M. Belen Oviedo,*[b,c] *Bryan M. Wong,*[b] *Christine M. Aikens*[a,*]

[a]Department of Chemistry, Kansas State University, Manhattan, Kansas 66506, United States

[b] Department of Chemical & Environmental Engineering and Materials Science & Engineering Program, University of California-Riverside, Riverside, California 92521, United States

[c]Instituto de Investigaciones Fisicoquímicas de Córdoba, Consejo Nacional de Investigaciones Científicas y Técnicas, Departamento de Química Teorica y Computacional, Facultad de Ciencias Químicas, Universidad Nacional de Córdoba, X5000HUA Córdoba, Argentina

AUTHOR INFORMATION

Corresponding Author

*cmaikens@ksu.edu, 1-785-532-0954, fax: 1-785-532-6666

ABSTRACT

Using real-time quantum dynamics calculations, we perform theoretical investigations of light-induced interactions and electronic excitation transfer in a silver nanoparticle dimer. Real-time time-dependent density functional tight-binding (RT-TDDFTB) calculations provide details of the quantum dynamical processes at an electronic/atomistic level with attosecond resolution. The computational efficiency of RT-TDDFTB allows us to examine electronic dynamics up to picosecond time scales. With time scales varying over six orders of magnitude, we provide insight into interactions between the nanoparticle and laser and between nanoparticles. Our results show that the coupling between nanoparticle monomers is dependent on the separation distance between the nanoparticles in the dimer. As the interparticle distance is varied, the dipole-dipole interactions and electronic excitation transfer mechanisms are markedly different. At large distances (from 50 to 20 Å), the energy transfer from NP1 to NP2 becomes more efficient as the interparticle distance decreases. The total dipole moment of the Ag_{14} nanoparticle dimer increases linearly at an interparticle distance of 20 Å and reaches its maximum after 1.2 ps. The electronic excitation transfer is also the most efficient at 20 Å. At short distances, back-transfer effects reduce the ability of the dimer and NP1 to accept energy from the incident electric field. We attribute the distance-dependent features of the nanoparticle dimer to the beating between the laser acting on NP1 and the back transfer from NP2 to NP1.

Introduction

The interaction between noble-metal nanoparticles and light have many applications in chemistry, physics, and biology. Due to their high physical and chemical stability,[1–4] noble-metal nanoparticles present a unique opportunity for exploring different properties and applications with tremendous tunability. One of the unique properties of these systems is the appearance of localized surface plasmon resonances (LSPRs).[5–10] LSPRs originate from the collective oscillation of free electrons of metal nanoparticles when excited by an external field. LSPRs enable high electric field intensities due to the plasmon resonance, high sensitivity to the environment, and strong interparticle coupling. In addition to the tunability of individual nanoparticles, the existence of neighboring particles can also modulate the optical properties of nanoparticle systems.[11–16]

The simplest model to study plasmonic coupling is the nanoparticle dimer. A systematic study of nanoparticle dimers not only provides more insight about nanoparticle interactions but also paves the way for further study of hybridized plasmons in more complex systems.[11,17,18] Beside hybridized plasmons, a large electromagnetic field enhancement can occur in a nanoparticle junction when the surface plasmon is excited. Studying nanoparticle dimers not only provides physical insights about nanoparticle interactions but also provides a deeper understanding of electromagnetic field enhancements.[16] The coherent nature of the LSPR results in large dipole moments, and electronic excitation transfer (EET) mechanisms can transfer energy to neighboring nanoparticles via electrostatic coupling. In previous experiments, Maier and co-workers observed EET from a localized source to a localized detector in a plasmon waveguide.[19] Yun et al. have used a noble nanocluster as an acceptor and reported EET with more than double the traditional Förster range.[20] The long-ranged nature of plasmonic interactions in EET has been analyzed by quantum dynamics calculations by Ilawe et al.[21] Investigations of electronic excitation transfer

mechanisms in nanoparticles at a quantum dynamical level of detail can provide insights for future applications in directing and controlling excitation energy in even more complex systems.[21–23]

Several previous theoretical studies have utilized density functional theory (DFT) and time-dependent density functional theory (TDDFT)[15,24–33] for describing quantum mechanical effects on optical properties.[34–36] Density functional tight-binding (DFTB)[37,38] and its real-time formalism (RT-TDDFTB)[21] are more computationally efficient for exploring large systems and longer time scales. Within the RT-TDDFTB formalism, the one-electron density matrix is propagated in the presence of an external electric field. The simulated optical absorption spectrum can be obtained by a Fourier transform of the time-evolving dipole moment into the frequency (energy) domain. Sanchez and co-workers have used RT-TDDFTB to investigate the relaxation dynamics of LSPRs in nanoclusters.[39–41] Wong and co-workers used RT-TDDFTB to study the electron dynamics of a plasmonic antenna for understanding plasmonic effects.[21–23] In addition to RT-TDDFTB, the linear response (LR) formalism of DFTB has also been used to calculate optical absorption spectra. In 2018, Alkan et al. used the LR-TDDFTB formalism to study the optical properties and electronic structures of silver nanorods and nanorod dimers.[13] Their results showed good agreement in the spectral shapes, energies, and intensity trends between the LR-TDDFT and LR-TDDFTB calculations. Liu et al. observed different absorption peak shifts in different sizes of homodimers and heterodimers, which are related to the direction of the transition dipole moment.[42]

Due to the high computational efficiency of DFTB and RT-TDDFTB, these methods can be used on simulations of large systems and long time scales. Moreover, because DFTB and RT-TDDFTB allow for the explicit treatment of electronic structure in the presence of external fields, they can more accurately predict electron dynamics effects compared to classical methods, particularly in cases where quantum mechanical effects become important. Quantum mechanical

methods are required to treat effects such as electron tunneling and charge transfer plasmons that emerge when the interparticle distance between nanoparticles becomes small. In this study, we employ RT-TDDFTB on a nanoparticle dimer system to examine each individual nanoparticle in the presence of an external electric field and understand the resulting dynamics as the distance between the nanoparticles is varied.

Computational Methods

The DFTB+ code[43] was used to calculate the ground-state Hamiltonian, overlap matrix elements, and the initial single-electron density matrix within the self-consistent density functional tight-binding (SCC-DFTB) formalism. SQUIRRELS (Streamlined QUantum Interface for Researching Real-Time ELectronic Systems),[21] a real-time implementation of DFTB, is used to probe the nonequilibrium electron dynamics. This methodology has also been used by other authors to compute the photoinjection dynamics in dye-sensitized TiO_2 solar cells,[44–46] excitation energy transfer in photosynthetic molecules,[47,48] in noncovalently bonded molecular aggregates,[49] many-body interactions in solvated nanodroplets,[23] and excitation energy transfer dynamics in plasmonic arrays.[21,22,36,50,51] Also, recently the implementation can be found in the DFTB+ code.[52] 250,000 electron dynamics steps were taken with a time step of 0.2 a.u. (4.8 attoseconds). Because of the computational efficiency of RT-TDDFTB, our simulations can be carried out to picoseconds with an attosecond time step, which spans over six orders of magnitude of time. We used a continuous wave field, which mimics a laser field polarized in the z direction, with an electric field strength of 0.0001 V/Angstrom. In our simulations, only the first Ag_{14} nanoparticle was excited with a laser, which was tuned to the highest excitation peak of the monomer (3.22 eV). The induced

dipole moment in the second Ag_{14} nanoparticle was due to stimulation from the first Ag_{14} nanoparticle.

For the quantum dynamics calculations, RT-TDDFTB propagates the one electron density matrix in the presence of an external time-varying electric field. The time-dependent Hamiltonian is given by:

$$H(t) = H^0 - E_0(t) \cdot \mu(t) \tag{1}$$

In equation (1), $\hat{H}^0$ is the reference Hamiltonian, $E_0(t)$ is the applied electric field, and $\hat{\mu}(t)$ is the dipole moment operator. In this work, the dipole moments are computed as:

$$\boldsymbol{\mu}(t) = e\sum_{i}^{N} q_i(t)\mathbf{r}_i \tag{2}$$

where e is the is the elementary charge, $\mathbf{r}_i$ is the cartesian coordinate of atom i and $q_i(t)$ is the Mulliken charge given by

$$q_i(t) = \sum_{\nu \in i}^{N} Z_\nu - (\rho S + S\rho)_{\nu\nu} \tag{3}$$

where Z_ν is the effective nuclear charge associated with atom i and the last term is a matrix element obtained by the product between the one-electron density matrix ρ and the overlap matrix S. In order to obtain the dipole moment of each NP in the dimer, we compute the Mulliken charge of each atom and then multiply by its cartesian coordinate and the elementary charge.

Because the quantum system propagates in the time domain, $E_0(t)$ can be chosen to take any time-dependent form. To simulate an optical absorption spectrum, $E_0(t)$ can be chosen as a

Dirac delta function and the absorption spectrum in the frequency domain can be obtained by a Fourier transform of the time-evolving dipole moment. To simulate the system interacting with monochromatic light, $E_0(t)$ can take the form of a sinusoidal perturbation. Different choices of the applied electric field give different but complementary viewpoints of quantum dynamics. According to the Liouville–von Neumann equation, upon interaction with time-dependent fields, the DFTB density matrix ρ will evolve as:[21,46]

$$\frac{\partial \rho}{\partial t} = \frac{1}{i\hbar}(S^{-1} \cdot H[\rho] \cdot \rho - \rho \cdot H[\rho] \cdot S^{-1}) \quad (4)$$

where H is the Hamiltonian matrix (which implicitly depends on the density matrix) and S is the overlap matrix.[21,46] The hyb-0-2 set of Slater-Koster parameters[53,54] for the silver atoms was used.

Two identical Ag_{14} were placed with different edge-to-edge interparticle distance (8, 9, 10, 12, 15, 20, 25, 30, 40, and 50 Å) as shown in Figure 1. These values correspond to the distances between the two closest atoms from different nanoparticles in the dimer structure along the z-axis. Only the first nanoparticle (donor) was excited with a laser (sinusoidal electric field perturbation) with its frequency equal to the monomer plasmonic energy (3.22 eV) and polarized along the intermolecular axis. Strong dipole moments are induced in the second nanoparticle (acceptor). The incident field is small enough (0.0001 V/Å) so that the system remains in the linear response regime. Based on previous work, we found an absorption peak of 3.2228 eV for the Ag_{14} monomer from LR-TDDFTB calculations,[42] which is resonant with a laser frequency of 3.22 eV used in our current work.

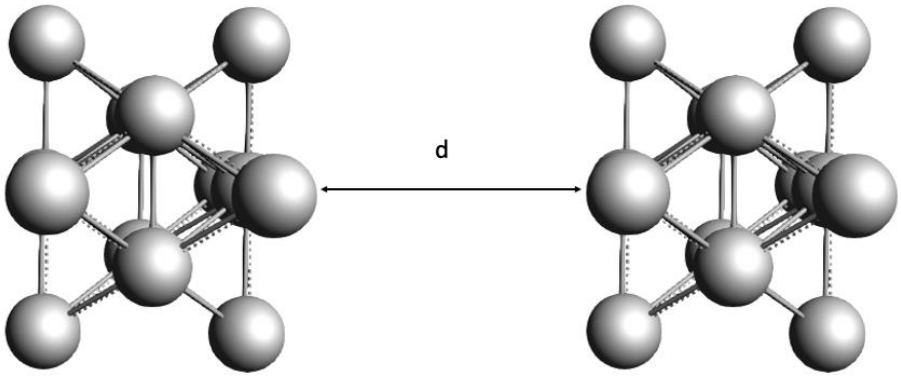

Figure 1. Interparticle distances between two identical Ag_{14} clusters.

Results and Discussion

Short-time dynamics

In our RT-TDDFTB study, initial excitation of NP1 in the z-direction leads to an increasing z-component of the dipole moment for NP1 followed by an induced dipole moment for NP2. The dipole moment components in the x and y direction are zero due to symmetry. In the short-time dynamics, the peak of the NP2 dipole moment occurs approximately when the NP1 dipole is zero, as shown in Figure 2. A previously formulated analytical model based on a two-level system (TLS)[55] is also used to analyze the nanoparticle dimer. Because the size of the Ag_{14} nanoparticles (face-to-face distance of 4 Å) is smaller than the interparticle distance (from 8 Å to 50 Å), we use a dipole approximation, which approximates the coupling between the nanoparticles as a point dipole interacting with another point dipole. In the analytical TLS, the dipole moment in NP2 is induced by the direct excitation of NP1. Based on linear response theory[56] and an analytical TLS, the dipole moment in NP1 can be expressed as:

$$\mu_1(t) \approx \frac{E_0}{\hbar} |\mu_1|^2 t \cdot \cos(\omega_{\mathrm{ex}} t)\, \hat{r} \tag{5}$$

where E_0 is the applied electric field, μ_1 is the transition dipole moment of NP1, $\omega_{ex} = \Delta E_{ex}/\hbar$ is the excitation energy, and $\hat{r}$ is the direction of the transition dipole moment.

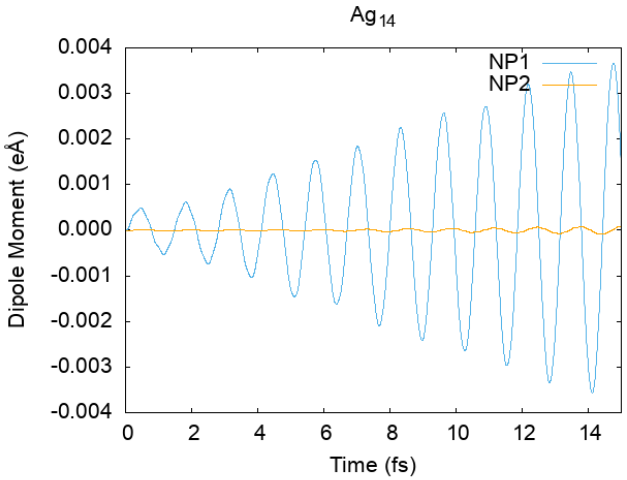

Figure 2. Short-time electron dynamics in our RT-TDDFTB simulation with an interparticle distance of 25 Å. The dipole moment of NP1 fluctuates under the external field, and the induced dipole moment of NP2 arises from the excitation of NP1.

Because both nanoparticles are identical, the transition dipole moment is the same. The induced dipole moment of NP2 in the homodimer system can be expressed as:

$$\mu_2(t) \approx -\frac{E_0}{4\pi\varepsilon_0\hbar^2 d^3}|\mu_1|^4 t^2 \sin(\omega_{\mathrm{ex}} t)\,\hat{r} \tag{6}$$

where ε_0 is the vacuum permittivity and d is the distance between the nanoparticles.

Long-time dynamics

From the TLS model, the peak of the dipole moment in NP1 increases linearly, which is expected because the energy constantly increases in a continuous laser field, while the peak of the dipole moment in NP2 increases quadratically as a function of time. These trends agree with short-time dynamics models. However, for longer times, we observe that the dipole moments of NP1 and NP2 deviate from this expectation. These deviations from the analytical model indicates the

complexity of long-time electron dynamics in nanoparticles. To understand these effects, we now analyze each individual nanoparticle system with different interparticle distances.

The computational efficiency of RT-TDDFTB allows us to simulate electronic dynamics up to picosecond time scales. The simulation for the nanoparticle dimer with a 50 Å separation is shown in Figure 3. Because the main interaction is dipolar, the peak of the dipole moment of NP1 increases linearly until 400 fs (Figure 3(b)), and the dipole moment of NP2 increases quadratically (Figure 3(c)), which agrees with the analytical TLS model for short-time dynamics as expected. For the first 700 fs, the dipole moment of the overall nanoparticle dimer mostly comes from NP1. Around 700 fs, the total dipole moment reaches its maximum, at which point NP2 contributes one-seventh of the dipole moment. After 700 fs, the contribution from NP1 decreases, while the contribution from NP2 still increases, although at a slower rate than before. The explanation for this phenomenon is that NP1 begins to transfer energy to NP2. Due to its oscillating dipole moment, NP1 creates an electric field that oscillates in time, which is then felt by NP2 because of the coupling between them. Even in this regime, with low coupling between the nanoparticles and a small incident field, the real-time simulations show that this system simulates EET of a plasmonic antenna.

As the interparticle distance of the dimer decreases to 40 Å (Figure 4), the overall profile of the dipole moment fluctuation is similar to the simulations with a 50 Å separation. However, the dipole moment intensity in NP2 is larger than that at the 50 Å separation, which indicates that EET from NP1 to NP2 becomes more efficient at 40 Å than at 50 Å. The total dipole moment reaches its maximum at 800 fs. Approximately one-third of its contribution comes from NP2, which is larger than its contribution for an interparticle distance of 50 Å. The linear increase in the dipole moment for NP1 deviates after 300 fs.

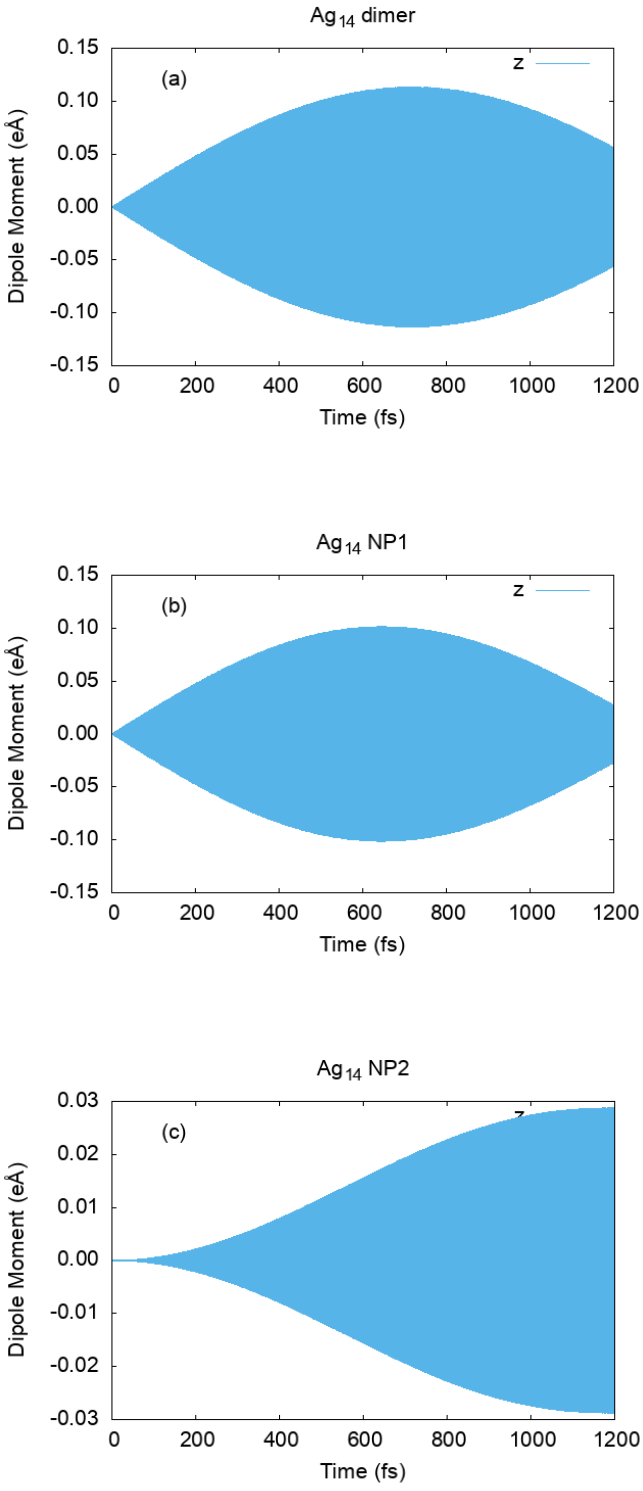

Figure 3. (a) Total dipole moment, (b) dipole moment of NP1, and (c) induced dipole moment of NP2 for a nanoparticle dimer with a 50 Å interparticle separation.

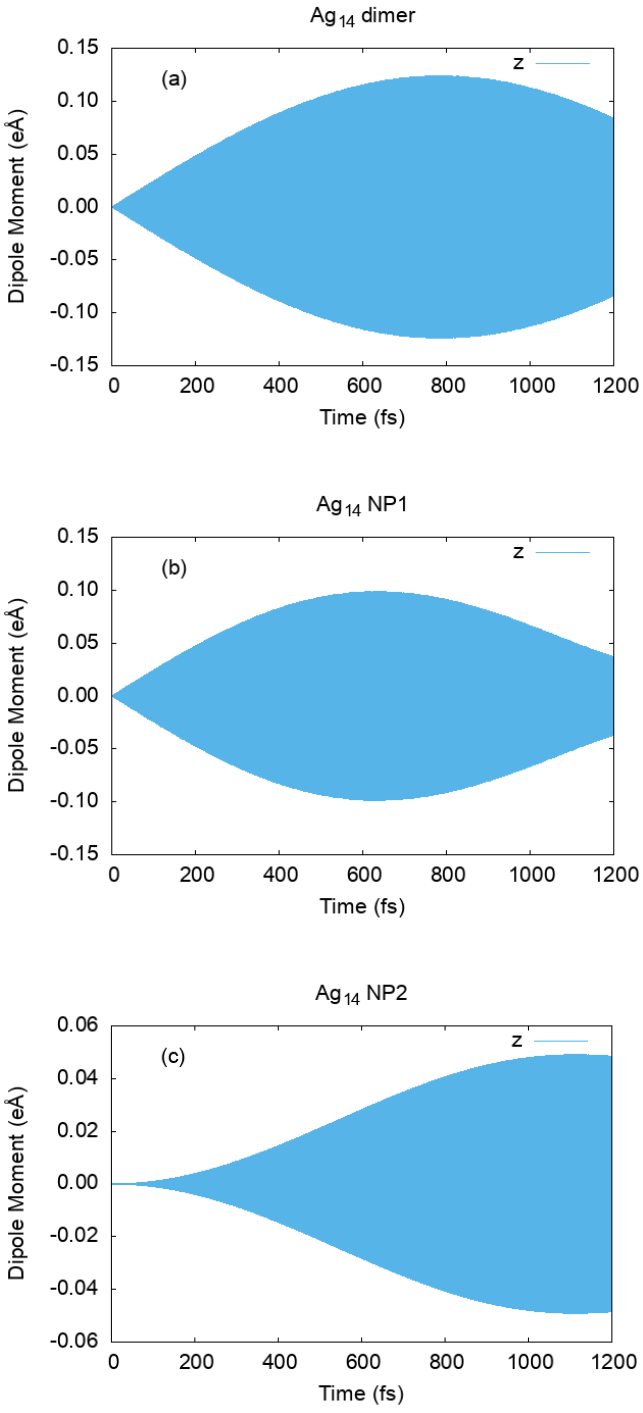

Figure 4. (a) Total dipole moment, (b) dipole moment of NP1, and (c) induced dipole moment of NP2 for a nanoparticle dimer with a 40 Å interparticle separation.

For the nanoparticle with an interparticle separation of 30 Å, the linear increase in the dipole moment for NP1 deviates after 200 fs. Around 1000 fs, the total dipole moment reaches its maximum. At a 30 Å separation, NP1 and NP2 have a nearly equal contribution to the total dipole moment after 600 fs. Comparing Figure 5(c) with Figure 3(c) and Figure 4(c), the induced dipole moment in NP2 for an interparticle distance of 30 Å is larger than the induced dipole moments for 50 and 40 Å. As shown in Figure 3(c), the induced dipole moment is around one-seventh of the total dipole moment in the dimer as shown in Figure 3(a). From Figure 4(c) and Figure 4(a), the contribution from NP2 is around one-third of the total. However, at a 30 Å separation, NP1 and NP2 have a similar contribution. An interesting phenomenon is observed here in the plasmon excitation of NP1. A plateau is noted between approximately 400-800 fs in which NP1 appears to have reached its maximum dipole moment arising from the incident electric field. Energy has been transferred to NP2, and the dipole moment of this second nanoparticle increases substantially. Then, the oscillating dipole moment of the second NP generates an electric field that induces an additional excitation to NP1. The EET to NP2 is more efficient at 30 Å than it is for 50 and 40 Å separations. At a smaller separation of 25 Å, the total dipole moment for the dimer (Figure 6(a)) is larger than the total dipole moment at longer distances of 50, 40, and 30 Å (Figures 3(a), 4(a), and 5(a), respectively), which indicates that energy transfer from the electric field to the dimer system is more efficient at an interparticle distance of 25 Å than at longer distances. In the range of interparticle separations from 25-50 Å, closer nanoparticles lead to more efficient EET.

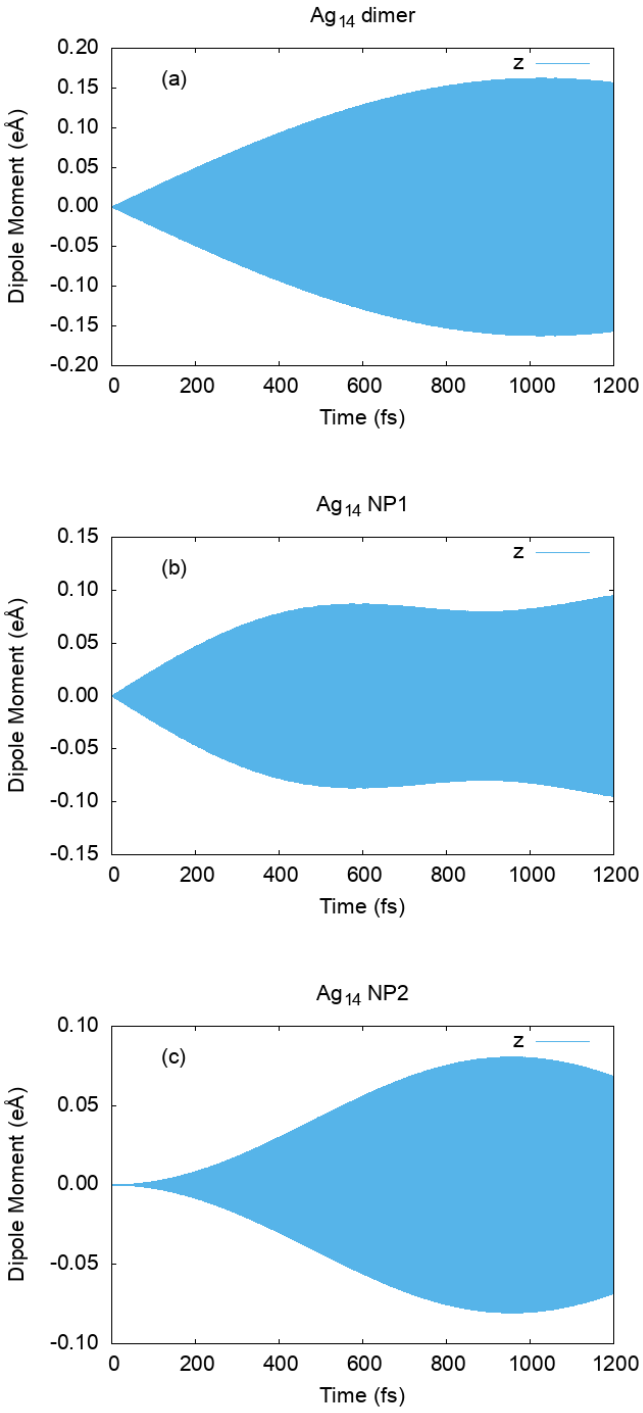

Figure 5. (a) Total dipole moment, (b) dipole moment of NP1, and (c) induced dipole moment of NP2 for a nanoparticle dimer with a 30 Å interparticle separation.

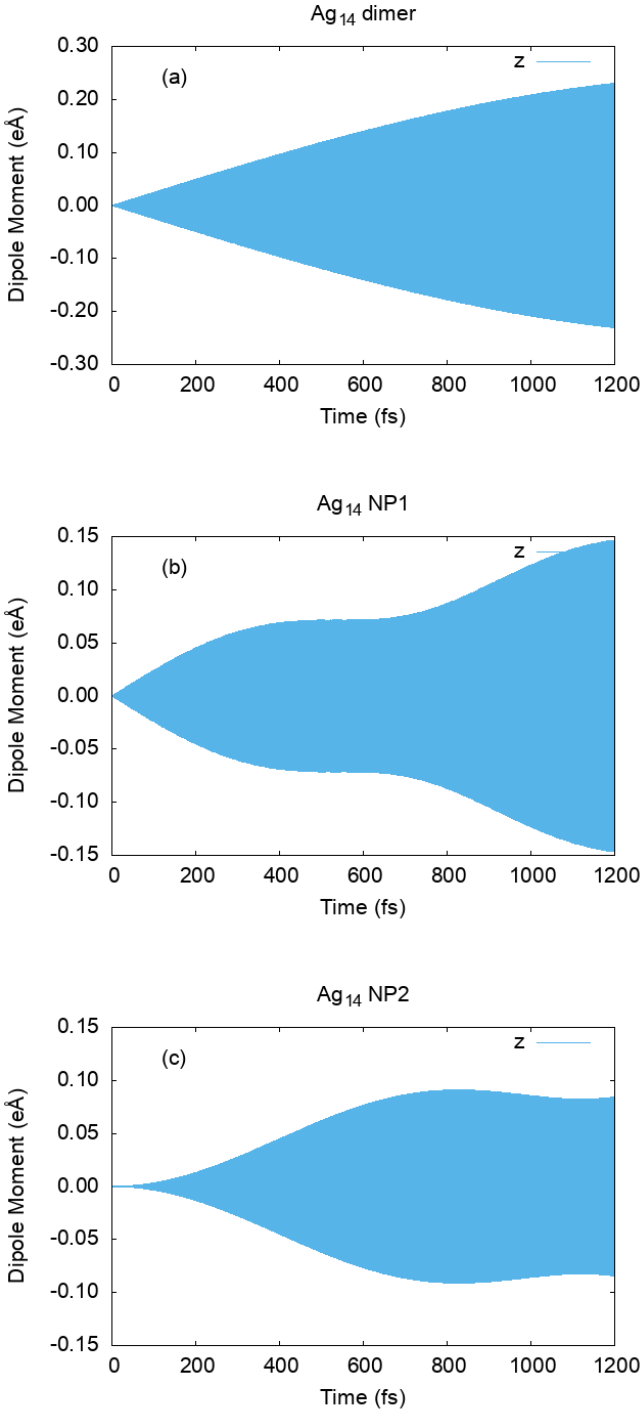

Figure 6. (a) Total dipole moment, (b) dipole moment of NP1, and (c) induced dipole moment of NP2 for a nanoparticle dimer with a 25 Å interparticle separation.

At a 20 Å interparticle distance, “wiggles” in the NP1 and NP2 dipole moments can be observed (Figure 7). However, the offset in phase between the two nanoparticles results in a linear increase in the total dipole moment. Again, oscillations in NP1 initially excite NP2, and the electric field that arises from the dipole oscillations in NP2 contribute to NP1. It should be noted that we do not have a bath in our calculations; the only route for energy transfer and/or electron transport is the coupling between NP1 and NP2. The dipole moment intensities for NP1 and NP2 are similar. Because the total dipole moment for the dimer is the largest out of all the different interparticle distances examined in this work, this dimer system is the most efficient at harvesting energy from the electric field compared to longer distances such as 50 Å, 40 Å, 30 Å, 25 Å and shorter distances, such as 15 Å and below, which we discuss below.

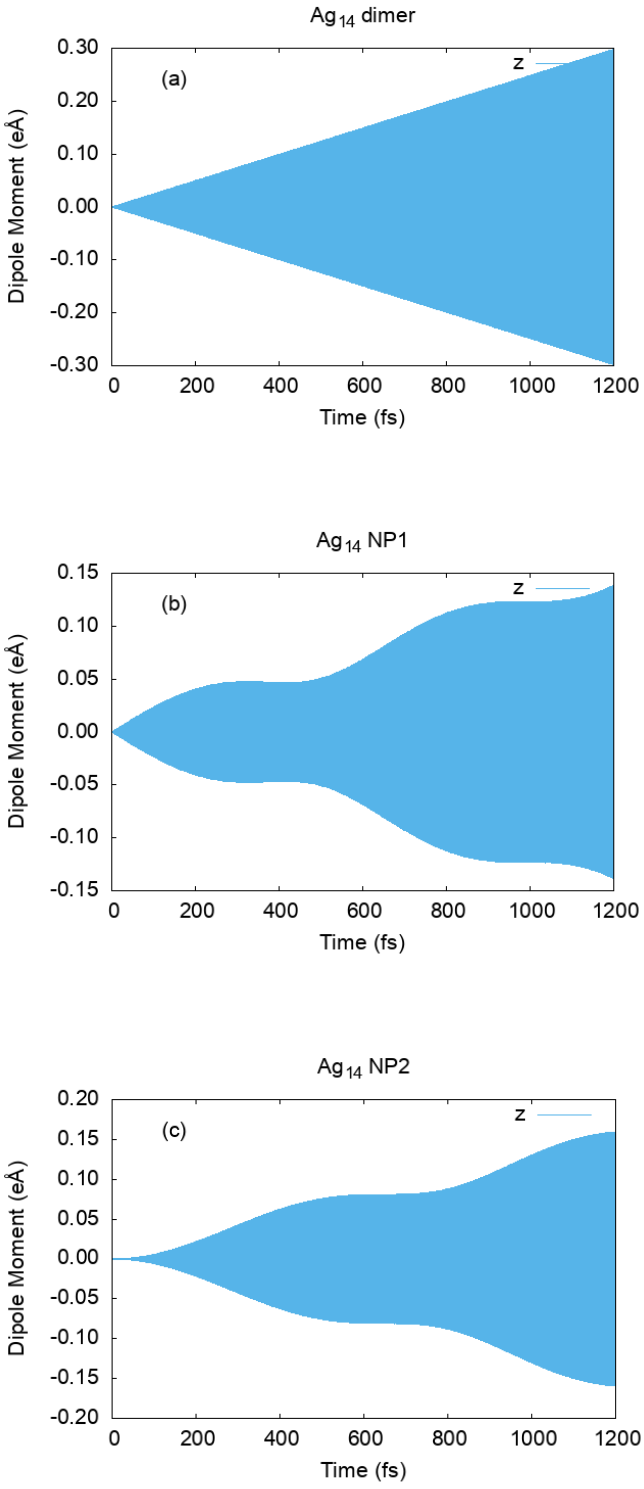

Figure 7. (a) Total dipole moment, (b) dipole moment of NP1, and (c) induced dipole moment of NP2 for a nanoparticle dimer with a 20 Å interparticle separation.

At a 15 Å separation distance, the total dipole moment is similar to that of 50 Å (Figure 8(a)); however, its origin is different. At a 50 Å interparticle distance, EET transfer is inefficient. The total dipole moment is mostly determined by the dipole moment of NP1. However, at a 15 Å interparticle distance, it is apparent that both NP1 and NP2 contribute substantially to the total dipole moment (Figures 8(b) and 8(c)). Examining the dipole moment profiles of NP1 and NP2 after 300 fs, the fluctuation in the magnitude of the dipole moment is out of phase for the two nanoparticles: as the dipole moment in NP2 increases, the dipole moment in NP1 decreases, and vice versa. The maximum of the total dipole moment occurs after 700 fs. The dipole moment intensities of both NP1 and NP2 show a decreasing trend after 700 fs. For NP1, the induced dipole moment from the electric field is less at larger interparticle distance, which indicates that back transfer[21,55] from NP2 to NP1 occurs and has a negative affect for NP1 harvesting energy from the electric field. From Equation (5) and Equation (6), the sinusoidal electric field will induce a dipole fluctuation with a $\cos(\omega_{ex}t)$ component. The $\cos(\omega_{ex}t)$ fluctuation of NP1 will induced a dipole fluctuation in NP2 with a component of $\sin(\omega_{ex}t)$. However, from back transfer from NP2 to NP1, we can expect a $\cos(\omega_{ex}t)$ component with the opposite sign.

From previous work,[21] the induced dipole moment from NP2 shows a d^{-6} distance dependence and t^3 time dependence. Thus, the back-transfer component should be proportional to d^{-6}. At short distances, the dipole moment fluctuates dramatically with minor changes in the interparticle distance. The t^3 factor indicates that the back transfer can also have a greater impact for longer time dynamics. Although this analytical model is limited, it succinctly explains the underlying physics in the RT-TDDFTB simulations.

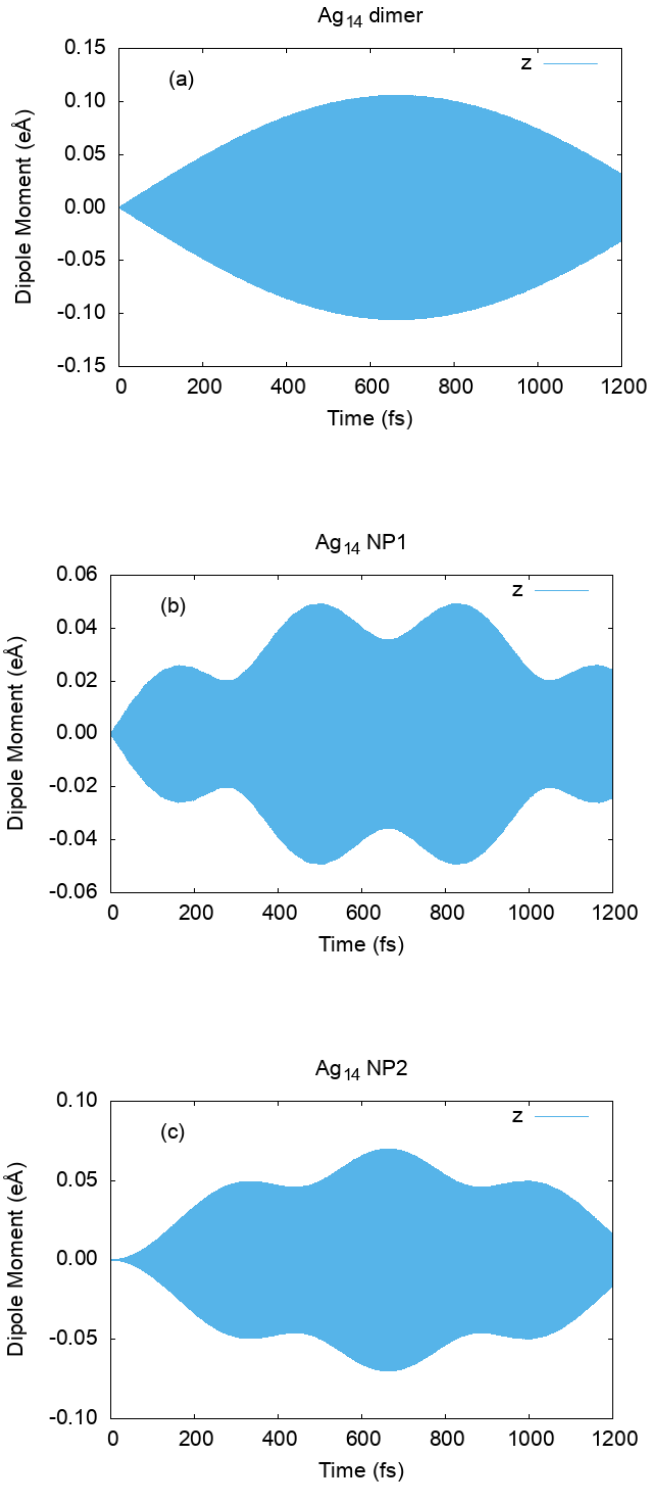

Figure 8. (a) Total dipole moment, (b) dipole moment of NP1, and (c) induced dipole moment of NP2 for a nanoparticle dimer with a 15 Å interparticle separation.

For a slightly smaller interparticle distance of 12 Å, one full cycle of the dipole moment fluctuation occurs near 600 fs (Figure 9). The total dipole moment and dipole moment of NP1 approaches zero, which indicates the back transfer from NP2 to NP1 is shielding NP1 from the electric field. However, the back transfer occurs earlier. From 0 to 100 fs, NP1 gains energy from the electric field and NP2 accepts energy from NP1. From 100 to 200 fs, the excitation energy transfer from NP1 to NP2 is larger than the energy transfer from the electric field to NP1, which leads to a decrease in the dipole moment from 100 to 200 fs for NP1 as shown in Figure 9(b). The back transfer reduces the ability of the dimer and NP1 to accept energy from the electric field. The maximum dipole moment intensity of the dimer is about half compared to its maximum intensity for the 15 Å separation, indicating the ability to harvest energy from the electric field has decreased. The dipole moment intensity of each individual nanoparticle is also halved compared to the respective energy for the 15 Å dimer.

From 10 to 8 Å (Figures 10-12), the overall dipole moment intensity of the dimer keeps decreasing as the interparticle distance in the dimer decreases. Within this distance range, the ability to harvest energy from the electric field also decreases. At short distances, the dipole moment of NP1 is smaller than NP2 due to back transfer from NP2 to NP1, reducing the energy absorption from the electric field. The oscillations and beating between back transfer and the laser acting on NP1 are even more pronounced as the interparticle distance decreases below 10 Å.

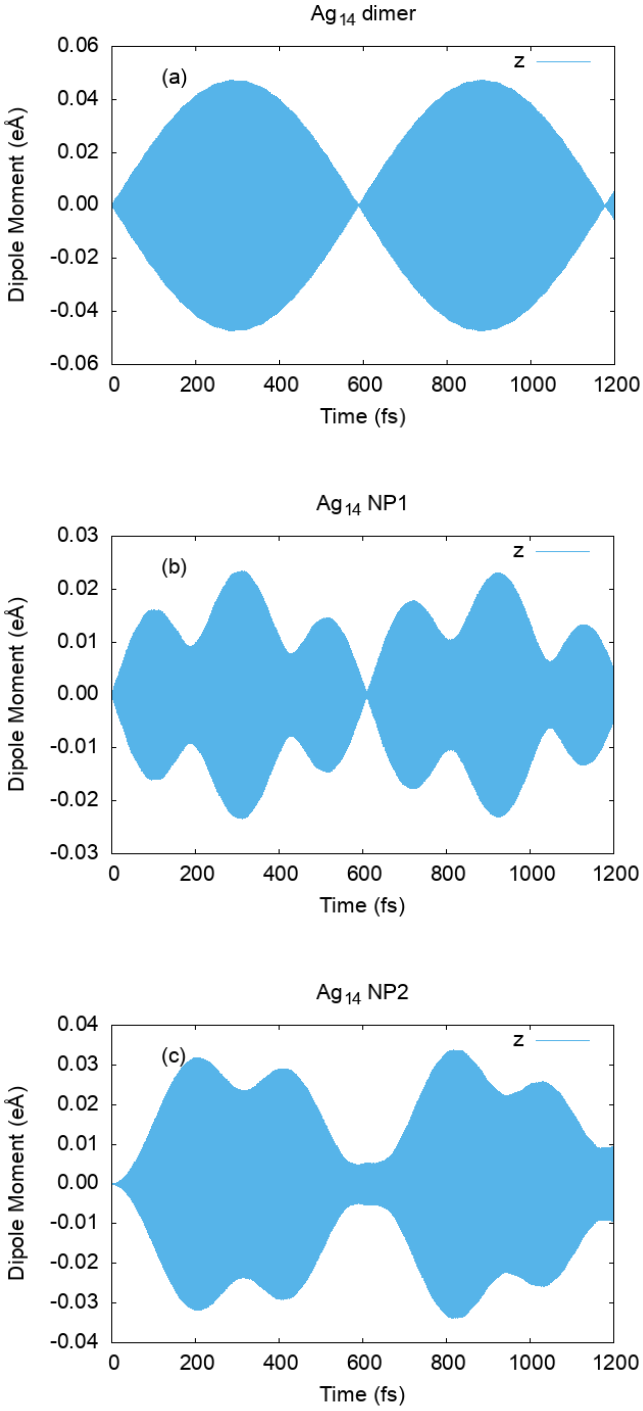

Figure 9. (a) Total dipole moment, (b) dipole moment of NP1, and (c) induced dipole moment of NP2 for a nanoparticle dimer with a 12 Å interparticle separation.

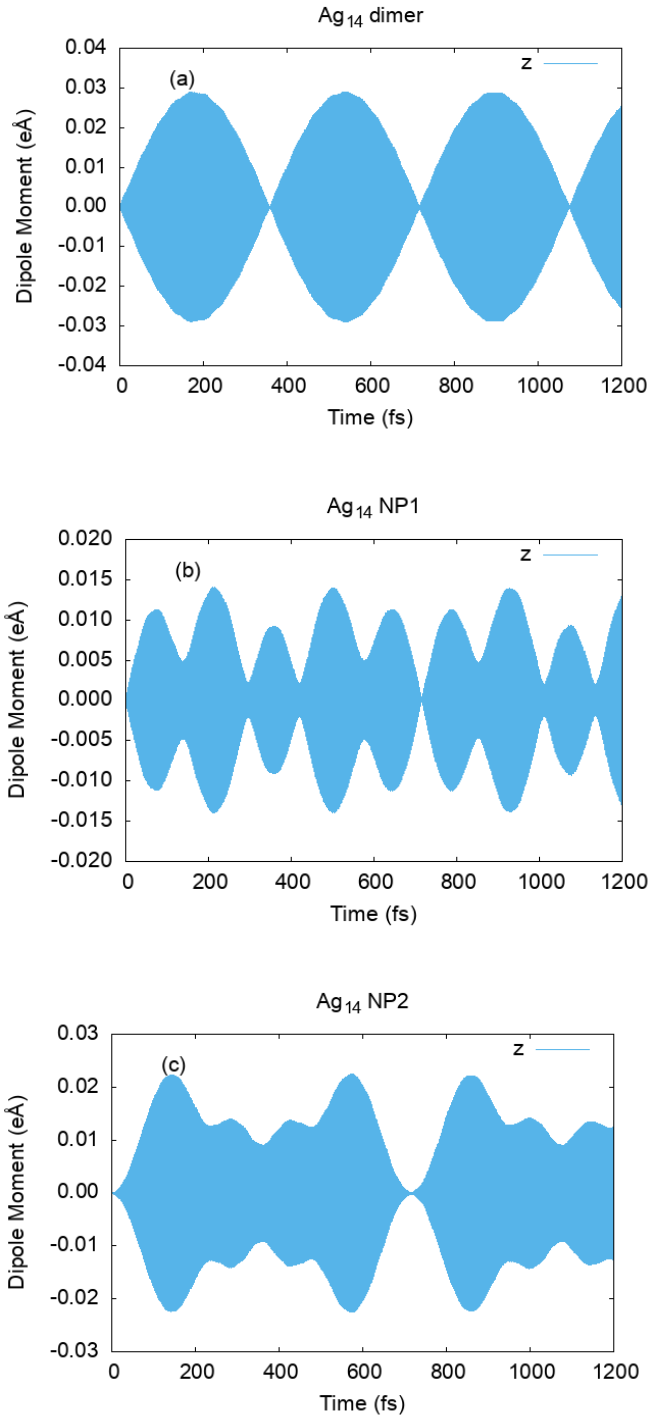

Figure 10. (a) Total dipole moment, (b) dipole moment of NP1, and (c) induced dipole moment of NP2 for a nanoparticle dimer with a 10 Å interparticle separation.

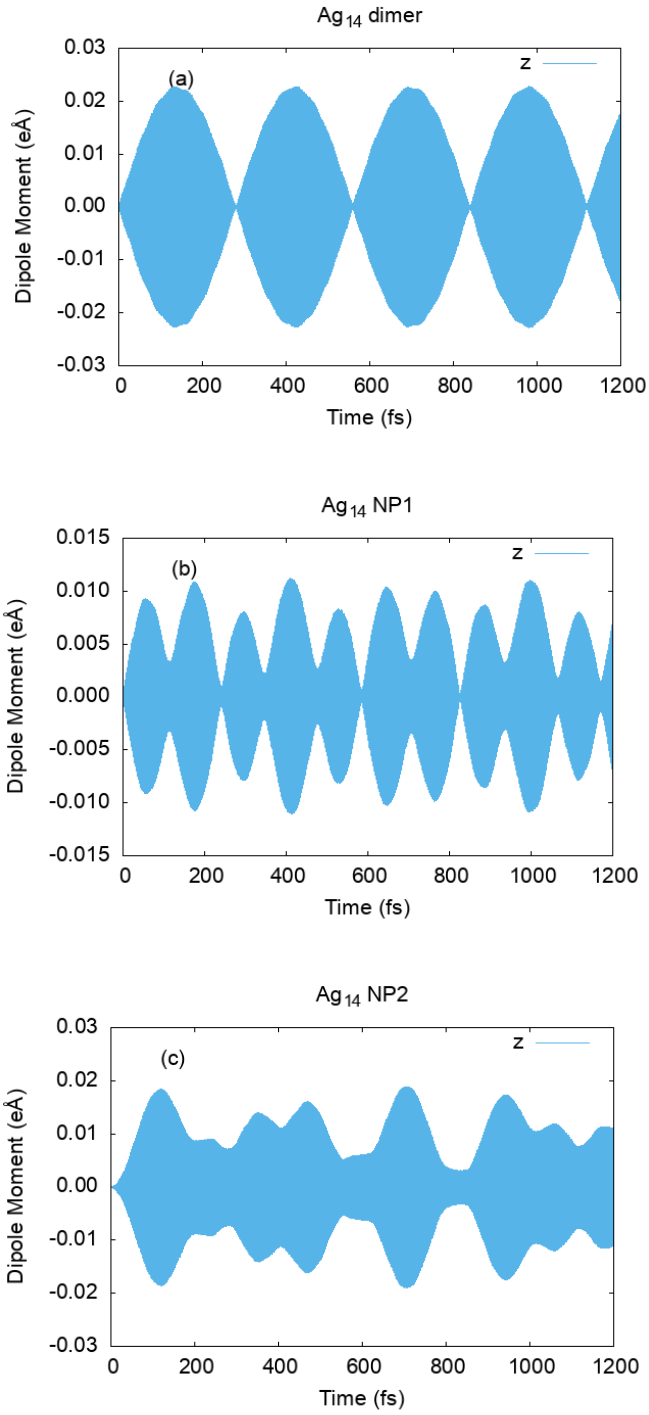

Figure 11. (a) Total dipole moment, (b) dipole moment of NP1, and (c) induced dipole moment of NP2 for a nanoparticle dimer with a 9 Å interparticle separation.

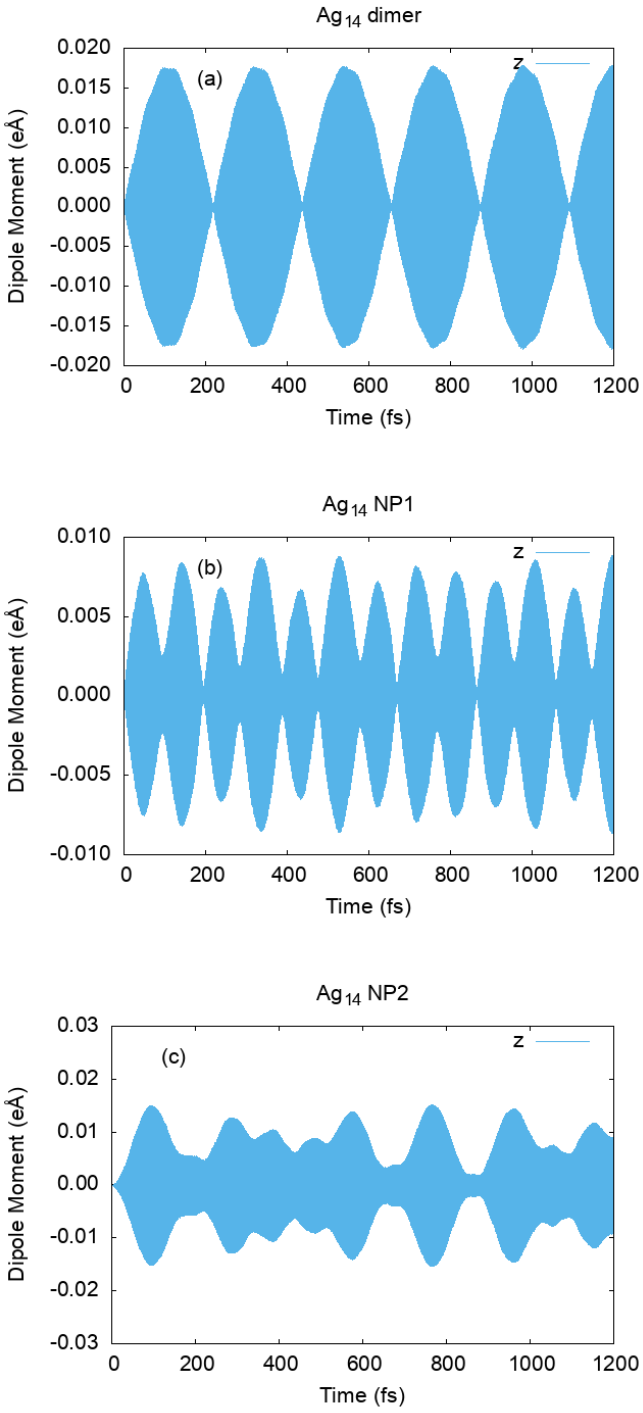

Figure 12. (a) Total dipole moment, (b) dipole moment of NP1, and (c) induced dipole moment of NP2 for a nanoparticle dimer with an 8 Å interparticle separation.

Based on these observations, we find that the dipole moment of the overall system has a sinusoidal envelope as a function of time, and the period of the overall oscillation envelope varies with interparticle distance. An exception occurs at 20 Å, which appears to exhibit a linear behavior for the total dipole moment. Based on the magnitude of the induced dipole moment for NP2, more energy can be transferred from NP1 to NP2 as the interparticle distance decreases towards 20 Å; in contrast, for distances below 20 Å, less energy transfers to NP2 since the induced dipole moment is smaller for distances smaller than 20 Å.

At 15 Å and below, numerous oscillations can be found in the individual dipole moments of NP1 and NP2. We observe that the period of oscillation arises due to "beating" between the back transfer from NP2 to NP1 and the laser energy acting on NP1. When the difference is small, the beating period is longer. For the 20 Å interparticle distance, the difference is approximately zero; as a result, the period of beating is approximately infinite, which can be seen as a linear increase in the total dipole moment.

Conclusions

In summary, using RT-TDDFTB, we simulated interactions of the Ag_{14} nanoparticle dimer with an incident sinusoidal electric field and examined the interaction between the individual nanoparticles and trends in the electronic excitation transfer with different distances. Due to the computational efficiency of RT-TDDFTB, we are able to simulate electronic dynamics at the picosecond time scale. Because the absorption of the incident electric field by one nanoparticle generates an electric field that oscillates in time, this induces a dipole moment oscillation in a second nanoparticle that is coupled to the original nanoparticle. These real-time calculations provide qualitative simulations of the EET occurring in plasmonic antenna systems. By analyzing the dipole moments of the dimer, as well as NP1 and NP2 individually, we found that all dipole

moments exhibit a unique dependence on the interparticle distance. At long interparticle distances, EET from NP1 to NP2 is not efficient. As this distance decreases, the dipole moment in NP2 changes significantly. The dipole moment of a dimer with a large interparticle distance arises mainly from NP1. At a 20 Å interparticle distance, the dipole moment of the dimer increases linearly due to the offset in phase between NP1 and NP2. The efficiency of the Ag_{14} dimer for gaining energy from the incident electric field is optimal at this distance. For shorter interparticle distances, back transfer can be observed, which has a strong dependence on distance and time. The back transfer from the RT-TDDFTB simulations shows a reduction in the ability of the dimer and NP1 to accept energy from the incident electric field when the interparticle distance is small. The dipole moment fluctuations in the Ag_{14} nanoparticle dimer (and both monomers) are affected by the laser acting on NP1, the energy transfer from NP1 to NP2, and the back transfer from NP2 to NP1. Our analyses and results provide additional mechanistic insight for controlling energy transfer effects by modulating interparticle distances and propagation times in these plasmonic systems.

Notes

Any additional relevant notes should be placed here.

The authors declare no competing financial interests.

ACKNOWLEDGMENT

This material is based on work supported by the Department of Energy under grant DE-SC0012273 to C.M.A. RT-TDDFTB analyses by B.M.W. were supported by the U.S. Department of Energy, Office of Science, Basic Energy Sciences, TCMP Program, under Award No. DE-SC0022209. We thank Dr. Fahri Alkan for helpful discussions.

REFERENCES

(1) Huang, X.; El-Sayed, I. H.; Qian, W.; El-Sayed, M. A. Cancer Cell Imaging and Photothermal Therapy in the Near-Infrared Region by Using Gold Nanorods. *J. Am. Chem. Soc.* **2006**, *128* (6), 2115–2120. https://doi.org/10.1021/ja057254a.

(2) Cognet, L.; Tardin, C.; Boyer, D.; Choquet, D.; Tamarat, P.; Lounis, B. Single Metallic Nanoparticle Imaging for Protein Detection in Cells. *Proceedings of the National Academy of Sciences* **2003**, *100* (20), 11350–11355. https://doi.org/10.1073/pnas.1534635100.

(3) Skirtach, A. G.; Dejugnat, C.; Braun, D.; Susha, A. S.; Rogach, A. L.; Parak, W. J.; Möhwald, H.; Sukhorukov, G. B. The Role of Metal Nanoparticles in Remote Release of Encapsulated Materials. *Nano Lett.* **2005**, *5* (7), 1371–1377. https://doi.org/10.1021/nl050693n.

(4) Nie, S. Probing Single Molecules and Single Nanoparticles by Surface-Enhanced Raman Scattering. *Science* **1997**, *275* (5303), 1102–1106. https://doi.org/10.1126/science.275.5303.1102.

(5) Yu; Chang, S.-S.; Lee, C.-L.; Wang, C. R. C. Gold Nanorods: Electrochemical Synthesis and Optical Properties. *J. Phys. Chem. B* **1997**, *101* (34), 6661–6664. https://doi.org/10.1021/jp971656q.

(6) Link, S.; El-Sayed, M. A. Spectral Properties and Relaxation Dynamics of Surface Plasmon Electronic Oscillations in Gold and Silver Nanodots and Nanorods. *J. Phys. Chem. B* **1999**, *103* (40), 8410–8426. https://doi.org/10.1021/jp9917648.

(7) Burda, C.; Chen, X.; Narayanan, R.; El-Sayed, M. A. Chemistry and Properties of Nanocrystals of Different Shapes. *Chem. Rev.* **2005**, *105* (4), 1025–1102. https://doi.org/10.1021/cr030063a.

(8) Eustis, S.; El-Sayed, M. A. Why Gold Nanoparticles Are More Precious than Pretty Gold: Noble Metal Surface Plasmon Resonance and Its Enhancement of the Radiative and Nonradiative Properties of Nanocrystals of Different Shapes. *Chem. Soc. Rev.* **2006**, *35* (3), 209–217. https://doi.org/10.1039/B514191E.

(9) Link, S.; Mohamed, M. B.; El-Sayed, M. A. Simulation of the Optical Absorption Spectra of Gold Nanorods as a Function of Their Aspect Ratio and the Effect of the Medium Dielectric Constant. *J. Phys. Chem. B* **1999**, *103* (16), 3073–3077. https://doi.org/10.1021/jp990183f.

(10) Guidez, E. B.; Aikens, C. M. Quantum Mechanical Origin of the Plasmon: From Molecular Systems to Nanoparticles. *Nanoscale* **2014**, *6* (20), 11512–11527. https://doi.org/10.1039/C4NR02225D.

(11) Nordlander, P.; Oubre, C.; Prodan, E.; Li, K.; Stockman, M. I. Plasmon Hybridizaton in Nanoparticle Dimers. *Nano Lett.* **2004**, *4*, 899.

(12) Aćimović, S. S.; Kreuzer, M. P.; González, M. U.; Quidant, R. Plasmon Near-Field Coupling in Metal Dimers as a Step toward Single-Molecule Sensing. *ACS Nano* **2009**, *3*, 1231.

(13) Alkan, F.; Aikens, C. M. TD-DFT and TD-DFTB Investigation of the Optical Properties and Electronic Structure of Silver Nanorods and Nanorod Dimers. *J. Phys. Chem. C* **2018**, *122* (41), 23639–23650. https://doi.org/10.1021/acs.jpcc.8b05196.

(14) Alkan, F.; Aikens, C. M. Understanding Plasmon Coupling in Nanoparticle Dimers Using Molecular Orbitals and Configuration Interaction. *Phys. Chem. Chem. Phys.* **2019**, *21* (41), 23065–23075. https://doi.org/10.1039/C9CP03890F.

(15) Bae, G. T.; Aikens, C. M. TDDFT and CIS Studies of Optical Properties of Dimers of Silver Tetrahedra. *J. Phys. Chem. A* **2012**, *116*, 8260.
(16) Marinica, D. C.; Kazansky, A. K.; Nordlander, P.; Aizpurua, J.; Borisov, A. G. Quantum Plasmonics: Nonlinear Effects in the Field Enhancement of a Plasmonic Nanoparticle Dimer. *Nano Lett.* **2012**, *12*, 1333.
(17) Prodan, E.; Radloff, C.; Halas, N. J.; Nordlander, P. A Hybridization Model for the Plasmon Response of Complex Nanostructures. *Science* **2003**, *302*, 419.
(18) Willingham, B.; Brandl, D. W.; Nordlander, P. Plasmon Hybridization in Nanorod Dimers. *Appl. Phys. B* **2008**, *93*, 209.
(19) Maier, S. A.; Kik, P. G.; Atwater, H. A.; Meltzer, S.; Harel, E.; Koel, B. E.; Requicha, A. A. G. Local Detection of Electromagnetic Energy Transport below the Diffraction Limit in Metal Nanoparticle Plasmon Waveguides. *Nature Mater* **2003**, *2* (4), 229–232. https://doi.org/10.1038/nmat852.
(20) Yun, C. S.; Javier, A.; Jennings, T.; Fisher, M.; Hira, S.; Peterson, S.; Hopkins, B.; Reich, N. O.; Strouse, G. F. Nanometal Surface Energy Transfer in Optical Rulers, Breaking the FRET Barrier. *J. Am. Chem. Soc.* **2005**, *127* (9), 3115–3119. https://doi.org/10.1021/ja043940i.
(21) Ilawe, N. V.; Oviedo, M. B.; Wong, B. M. Real-Time Quantum Dynamics of Long-Range Electronic Excitation Transfer in Plasmonic Nanoantennas. *J. Chem. Theory Comput.* **2017**, *13*, 3442.
(22) Ilawe, N. V.; Oviedo, M. B.; Wong, B. M. Effect of Quantum Tunneling on the Efficiency of Excitation Energy Transfer in Plasmonic Nanoparticle Chain Waveguides. *J. Mater. Chem. C* **2018**, *6* (22), 5857–5864. https://doi.org/10.1039/C8TC01466C.
(23) Oviedo, M. B.; Wong, B. M. Real-Time Quantum Dynamics Reveals Complex, Many-Body Interactions in Solvated Nanodroplets. *J. Chem. Theory Comput.* **2016**, *12* (4), 1862–1871. https://doi.org/10.1021/acs.jctc.5b01019.
(24) Aikens, C. M.; Li, S. Z.; Schatz, G. C. From Discrete Electronic States to Plasmons: TDDFT Optical Absorption Properties of Agn (n = 10, 20, 35, 56, 84, 120) Tetrahedral Clusters. *J. Phys. Chem. C* **2008**, *112*, 11272.
(25) Johnson, H. E.; Aikens, C. A. Electronic Structure and TDDFT Optical Absorption Spectra of Silver Nanorods. *J. Phys. Chem. A* **2009**, *113*, 4445.
(26) Guidez, E. B.; Aikens, C. M. Diameter Dependence of the Excitation Spectra of Silver and Gold Nanorods. *J. Phys. Chem. C* **2013**, *117*, 12325.
(27) Stener, M.; Nardelli, A.; De Francesco, R.; Fronzoni, G. Optical Excitations of Gold Nanoparticles: A Quantum Chemical Scalar Relativistic Time Dependent Density Functional Study. *J. Phys. Chem. C* **2007**, *111*, 11862.
(28) Durante, N.; Fortunelli, A.; Broyer, M.; Stener, M. Optical Properties of Au Nanoclusters from TD-DFT Calculations. *J. Phys. Chem. C* **2011**, *115*, 6277.
(29) Barcaro, G.; Sernenta, L.; Fortunelli, A.; Stener, M. Optical Properties of Silver Nanoshells from Time-Dependent Density Functional Theory Calculations. *J. Phys. Chem. C* **2014**, *118*, 12450.
(30) Weissker, H. C.; Mottet, C. Optical Properties of Pure and Core-Shell Noble-Metal Nanoclusters from TDDFT: The Influence of the Atomic Structure. *Phys. Rev. B* **2011**, *84*, 165443.

(31) López-Lozano, X.; Barron, H.; Mottet, C.; Weissker, H.-C. Aspect-Ratio- and Size-Dependent Emergence of the Surface-Plasmon Resonance in Gold Nanorods – an Ab Initio TDDFT Study. *Phys. Chem. Chem. Phys.* **2014**, *16*, 1820.

(32) Liao, M. S.; Bonifassi, P.; Leszczynski, J.; Ray, P. C.; Huang, M. J.; Watts, J. D. Structure, Bonding, and Linear Optical Properties of a Series of Silver and Gold Nanorod Clusters: DFT/TDDFT Studies. *J. Phys. Chem. A* **2010**, *114*, 12701.

(33) Iida, K.; Noda, M.; Ishimura, K.; Nobusada, K. First-Principles Computational Visualization of Localized Surface Plasmon Resonance in Gold Nanoclusters. *J. Phys. Chem. A* **2014**, *118*, 11317.

(34) Asadi-Aghbolaghi, N.; Rüger, R.; Jamshidi, Z.; Visscher, L. TD-DFT+TB: An Efficient and Fast Approach for Quantum Plasmonic Excitations. *J. Phys. Chem. C* **2020**, *124* (14), 7946–7955. https://doi.org/10.1021/acs.jpcc.0c00979.

(35) D'Agostino, S.; Rinaldi, R.; Cuniberti, G.; Della Sala, F. Density Functional Tight Binding for Quantum Plasmonics. *J. Phys. Chem. C* **2018**, *122* (34), 19756–19766. https://doi.org/10.1021/acs.jpcc.8b05278.

(36) Douglas-Gallardo, O. A.; Berdakin, M.; Frauenheim, T.; Sánchez, C. G. Plasmon-Induced Hot-Carrier Generation Differences in Gold and Silver Nanoclusters. *Nanoscale* **2019**, *11* (17), 8604–8615. https://doi.org/10.1039/C9NR01352K.

(37) Porezag, D.; Frauenheim, T.; Kohler, T.; Seifert, G.; Kaschner, R. Construction of Tight-Binding-Like Potentials on the Basis of Density-Functional Theory – Application to Carbon. *Phys. Rev. B* **1995**, *51*, 12947.

(38) Seifert, G.; Porezag, D.; Frauenheim, T. Calculations of Molecules, Clusters, and Solids with a Simplified LCAO-DFT-LDA Scheme. *Int. J. Quantum Chem.* **1996**, *58*, 185.

(39) Douglas-Gallardo, O. A.; Berdakin, M.; Sanchez, C. G. Atomistic Insights into Chemical Interface Damping of Surface Plasmon Excitations in Silver Nanoclusters. *J. Phys. Chem. C* **2016**, *120*, 24389.

(40) Bonafé, F. P.; Aradi, B.; Guan, M. X.; Douglas-Gallardo, O. A.; Lian, C.; Meng, S.; Frauenheim, T.; Sánchez, C. G. Plasmon-Driven Sub-Picosecond Breathing of Metal Nanoparticles. *Nanoscale* **2017**, *9*, 12391.

(41) Douglas-Gallardo, O. A.; Soldano, G. J.; Mariscal, M. M.; Sanchez, C. G. Effects of Oxidation on the Plasmonic Properties of Aluminum Nanoclusters. *Nanoscale* **2017**, *9*, 17471.

(42) Liu, Z.; Alkan, F.; Aikens, C. M. TD-DFTB Study of Optical Properties of Silver Nanoparticle Homodimers and Heterodimers. *J. Chem. Phys.* **2020**, *153* (14), 144711. https://doi.org/10.1063/5.0025672.

(43) Aradi, B.; Hourahine, B.; Frauenheim, Th. DFTB+, a Sparse Matrix-Based Implementation of the DFTB Method. *J. Phys. Chem. A* **2007**, *111* (26), 5678–5684. https://doi.org/10.1021/jp070186p.

(44) Negre, C. F. A.; Fuertes, V. C.; Oviedo, M. B.; Oliva, F. Y.; Sánchez, C. G. Quantum Dynamics of Light-Induced Charge Injection in a Model Dye–Nanoparticle Complex. *J. Phys. Chem. C* **2012**, *116* (28), 14748–14753. https://doi.org/10.1021/jp210248k.

(45) Oviedo, M. B.; Zarate, X.; Negre, C. F. A.; Schott, E.; Arratia-Pérez, R.; Sánchez, C. G. Quantum Dynamical Simulations as a Tool for Predicting Photoinjection Mechanisms in Dye-Sensitized TiO_2 Solar Cells. *J. Phys. Chem. Lett.* **2012**, *3* (18), 2548–2555. https://doi.org/10.1021/jz300880d.

(46) Negre, C. F. A.; Young, K. J.; Oviedo, Ma. B.; Allen, L. J.; Sánchez, C. G.; Jarzembska, K. N.; Benedict, J. B.; Crabtree, R. H.; Coppens, P.; Brudvig, G. W.; Batista, V. S. Photoelectrochemical Hole Injection Revealed in Polyoxotitanate Nanocrystals Functionalized with Organic Adsorbates. *J. Am. Chem. Soc.* **2014**, *136* (46), 16420–16429. https://doi.org/10.1021/ja509270f.

(47) Oviedo, M. B.; Negre, C. F. A.; Sánchez, C. G. Dynamical Simulation of the Optical Response of Photosynthetic Pigments. *Phys. Chem. Chem. Phys.* **2010**, *12* (25), 6706. https://doi.org/10.1039/b926051j.

(48) Oviedo, M. B.; Sánchez, C. G. Transition Dipole Moments of the Q_y Band in Photosynthetic Pigments. *J. Phys. Chem. A* **2011**, *115* (44), 12280–12285. https://doi.org/10.1021/jp203826q.

(49) Medrano, C. R.; Oviedo, M. B.; Sánchez, C. G. Photoinduced Charge-Transfer Dynamics Simulations in Noncovalently Bonded Molecular Aggregates. *Phys. Chem. Chem. Phys.* **2016**, *18* (22), 14840–14849. https://doi.org/10.1039/C6CP00231E.

(50) Ilawe, N. V.; Oviedo, M. B.; Wong, B. M. Correction to Real-Time Quantum Dynamics of Long-Range Electronic Excitation Transfer in Plasmonic Nanoantennas. *J. Chem. Theory Comput.* **2017**, *13* (12), 6433–6433. https://doi.org/10.1021/acs.jctc.7b01150.

(51) Berdakin, M.; Douglas-Gallardo, O. A.; Sánchez, C. G. Interplay between Intra- and Interband Transitions Associated with the Plasmon-Induced Hot Carrier Generation Process in Silver and Gold Nanoclusters. *J. Phys. Chem. C* **2020**, *124* (2), 1631–1639. https://doi.org/10.1021/acs.jpcc.9b10871.

(52) Hourahine, B.; Aradi, B.; Blum, V.; Bonafé, F.; Buccheri, A.; Camacho, C.; Cevallos, C.; Deshaye, M. Y.; Dumitrică, T.; Dominguez, A.; Ehlert, S.; Elstner, M.; van der Heide, T.; Hermann, J.; Irle, S.; Kranz, J. J.; Köhler, C.; Kowalczyk, T.; Kubař, T.; Lee, I. S.; Lutsker, V.; Maurer, R. J.; Min, S. K.; Mitchell, I.; Negre, C.; Niehaus, T. A.; Niklasson, A. M. N.; Page, A. J.; Pecchia, A.; Penazzi, G.; Persson, M. P.; Řezáč, J.; Sánchez, C. G.; Sternberg, M.; Stöhr, M.; Stuckenberg, F.; Tkatchenko, A.; Yu, V. W. -z.; Frauenheim, T. DFTB+, a Software Package for Efficient Approximate Density Functional Theory Based Atomistic Simulations. *J. Chem. Phys.* **2020**, *152* (12), 124101. https://doi.org/10.1063/1.5143190.

(53) Szűcs, B.; Hajnal, Z.; Frauenheim, T.; Gonzalez, C.; Ortega, J.; Perez, R.; Flores, F. Chalcogen Passivation of GaAs(100) Surfaces: Theoretical Study. *Appl. Surf. Sci.* **2003**, *212–213*, 861.

(54) Szűcs, B.; Hajnal, Z.; Scholz, R.; Sanna, S.; Frauenheim, T. Theoretical Study of the Adsorption of a PTCDA Monolayer on S-Passivated GaAs(100). *Appl. Surf. Sci.* **2004**, *234*, 173.

(55) Oviedo, M. B.; Sánchez, C. G. Full Quantum Dynamics of the Electronic Coupling between Photosynthetic Pigments. *arXiv:1502.00491 [cond-mat, physics:physics]* **2015**.

(56) Mukamel, S. Principles of Nonlinear Optical Spectroscopy; 1995.

Accepted to J. Chem. Phys. 10.1063/5.0082960

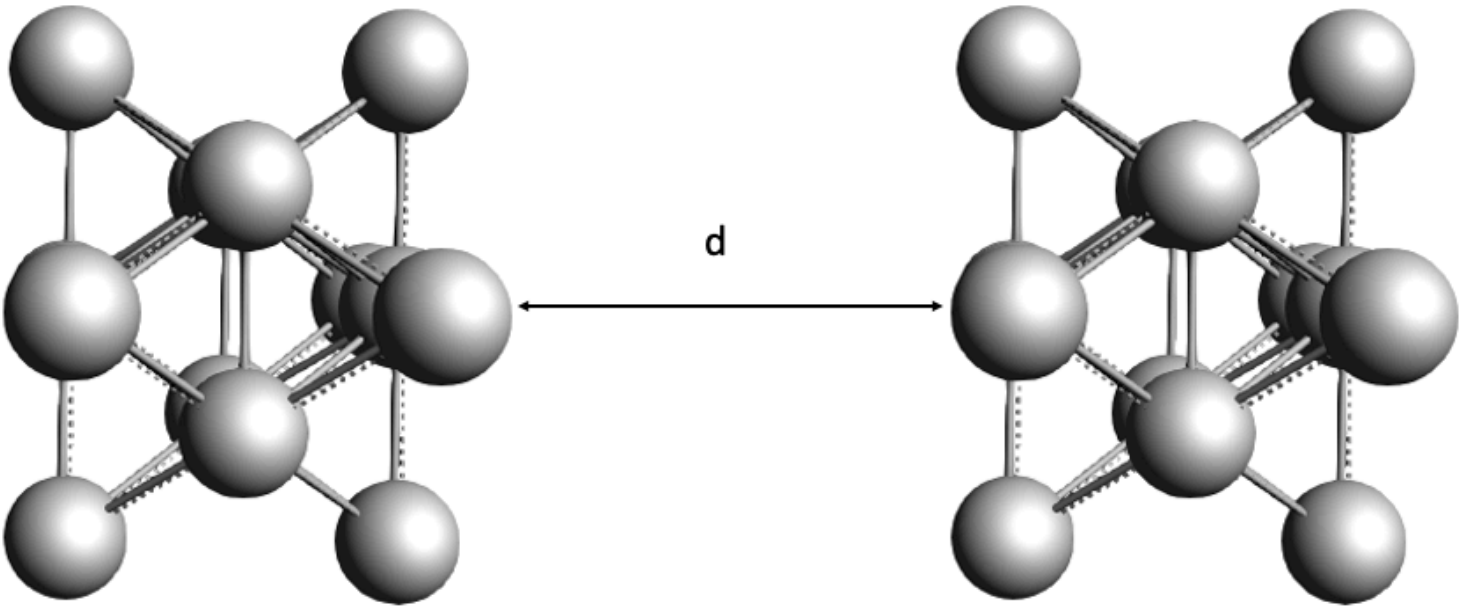

Accepted to J. Chem. Phys. 10.1063/5.0082960

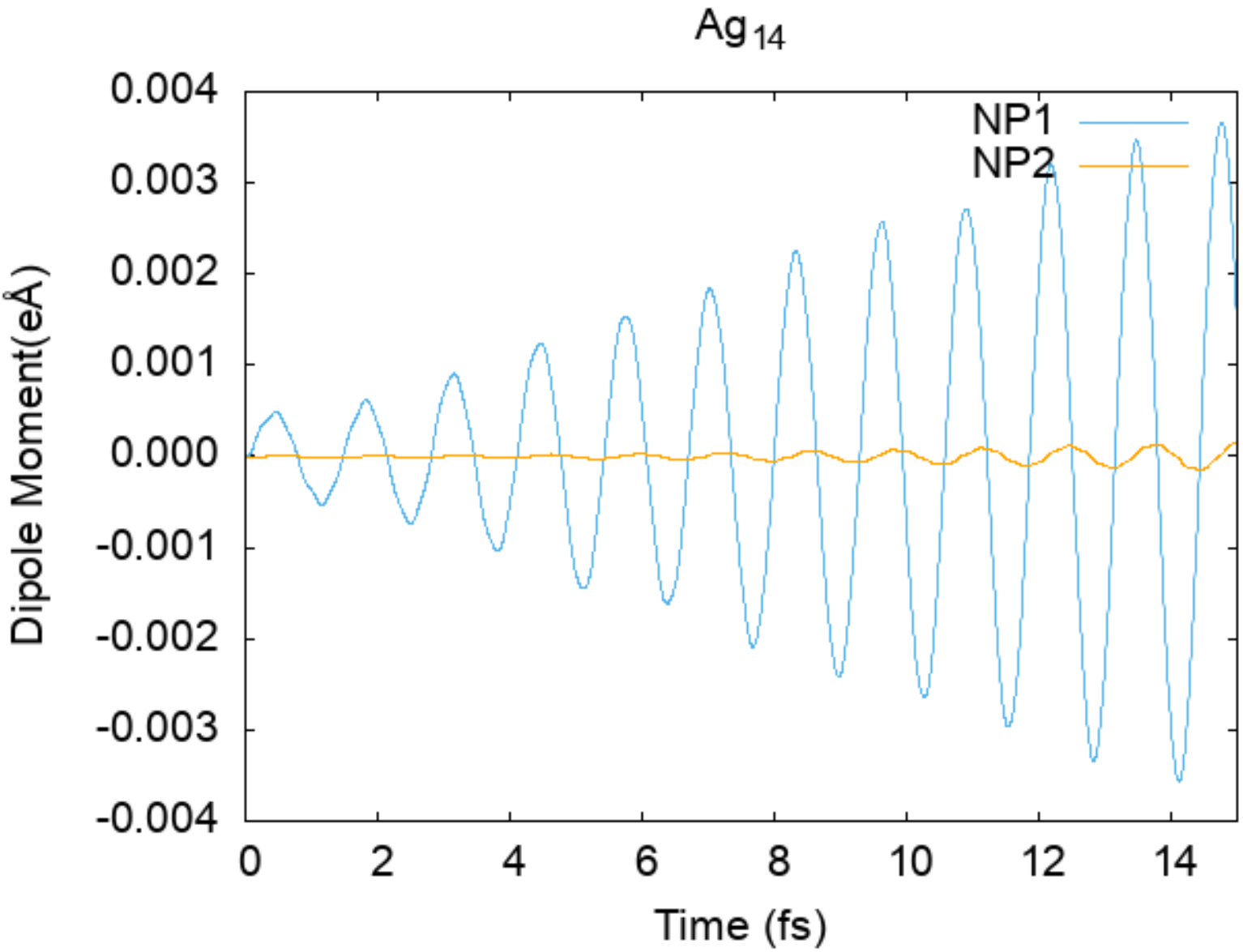

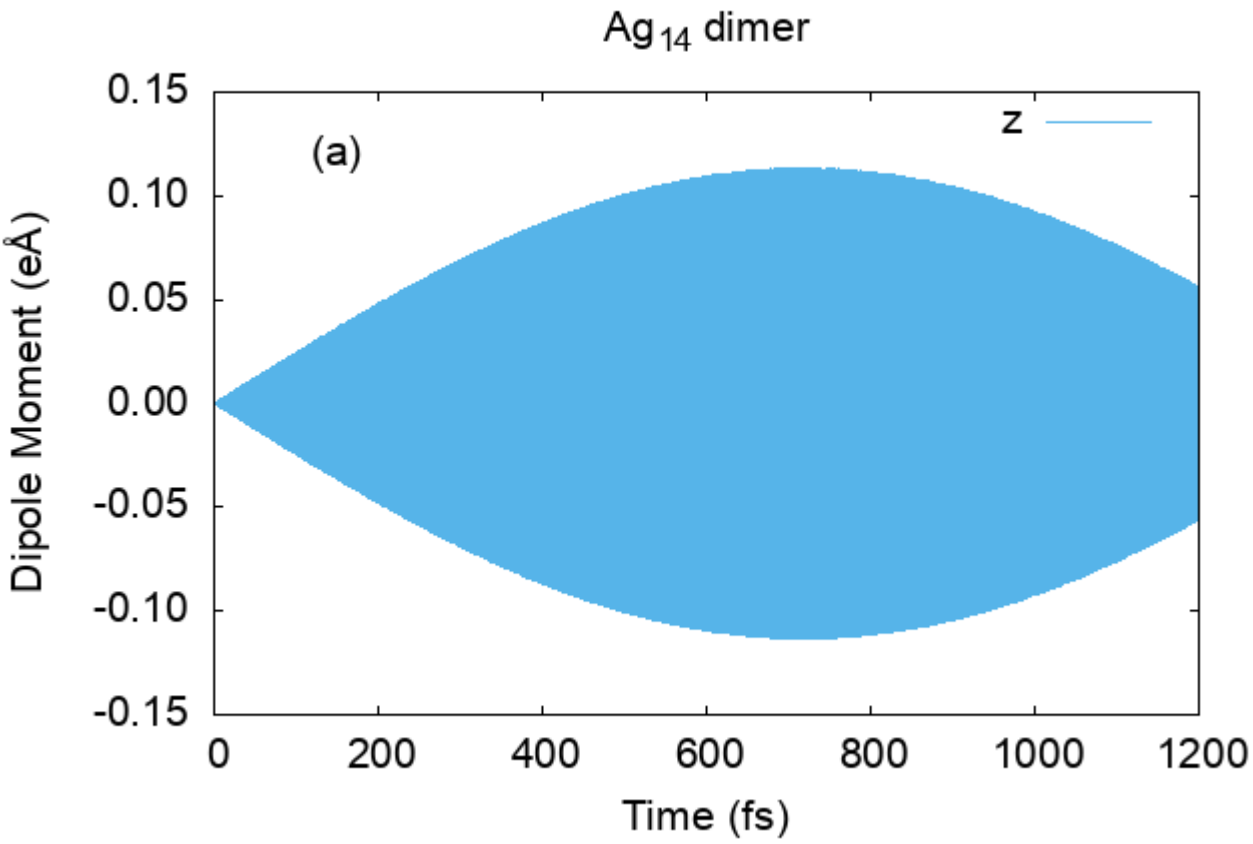
Ag 14 dimer
(a)
z
Dipole Moment (eÅ)
0.15
0.10
0.05
0.00
-0.05
-0.10
-0.15
0
200
400
600
800
1000
1200
Time (fs)

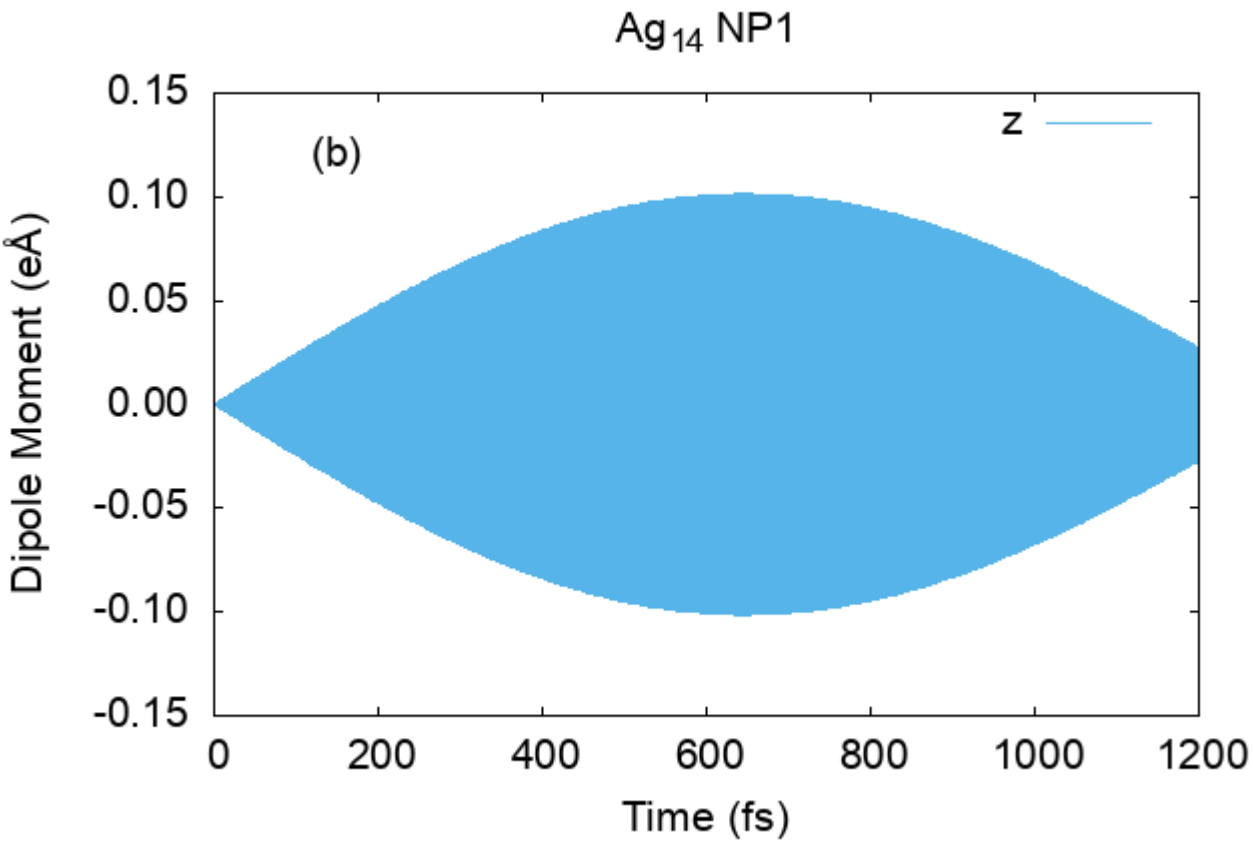
Ag 14 NP1
(b)
z
Dipole Moment (eÅ)
0.15
0.10
0.05
0.00
-0.05
-0.10
-0.15
0
200
400
600
800
1000
1200
Time (fs)

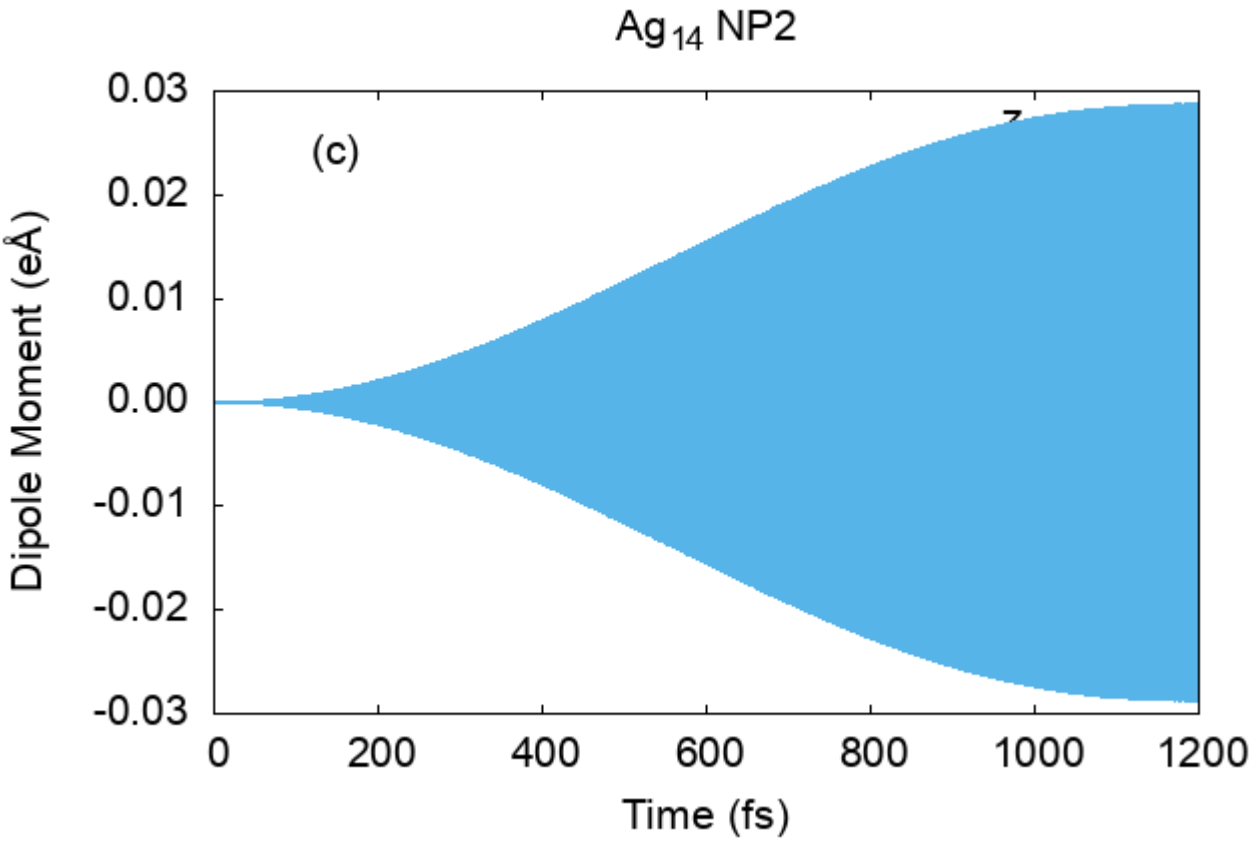
Ag 14 NP2
(c)
Dipole Moment (eÅ)
0.03
0.02
0.01
0.00
-0.01
-0.02
-0.03
0
200
400
600
800
1000
1200
Time (fs)

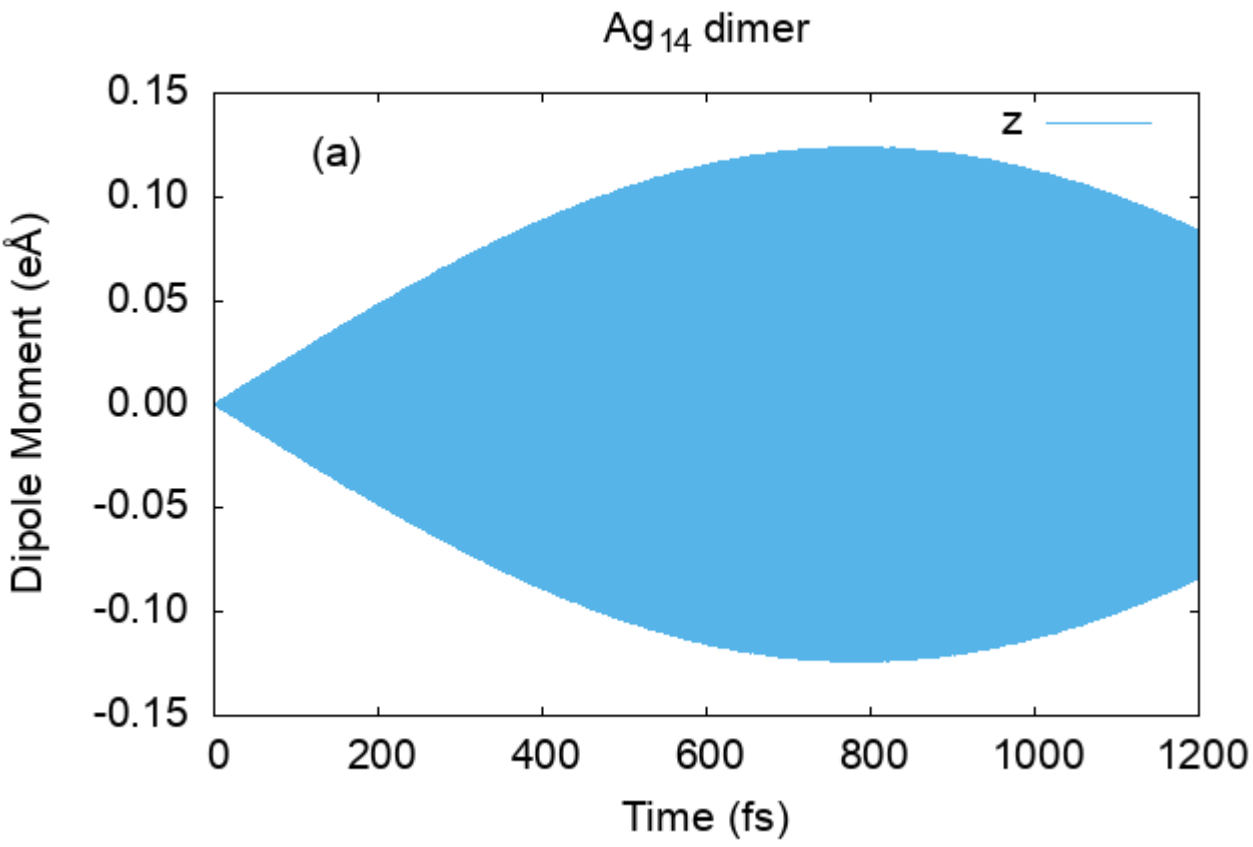
Ag 14 dimer
(a)
z
Dipole Moment (eÅ)
0.15
0.10
0.05
0.00
-0.05
-0.10
-0.15
0
200
400
600
800
1000
1200
Time (fs)

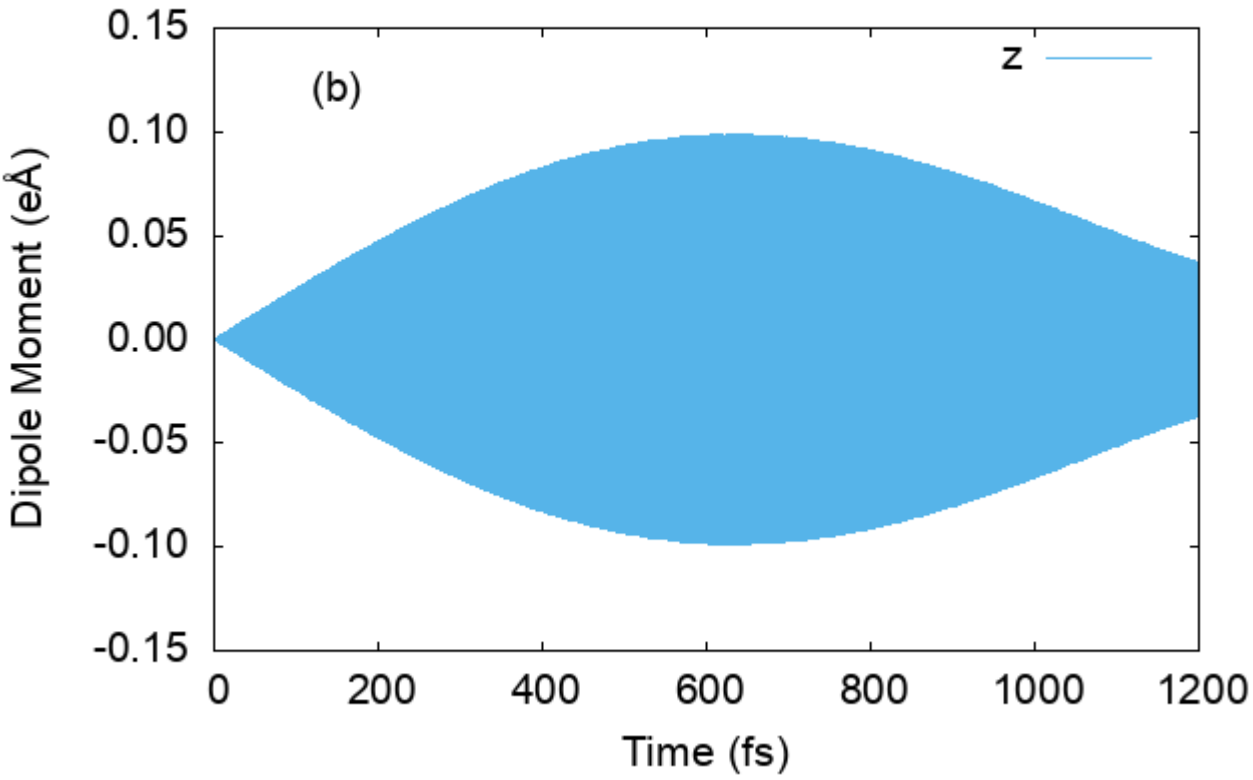
Ag 14 NP1
(b)
z
Dipole Moment (eÅ)
0.15
0.10
0.05
0.00
-0.05
-0.10
-0.15
0
200
400
600
800
1000
1200
Time (fs)

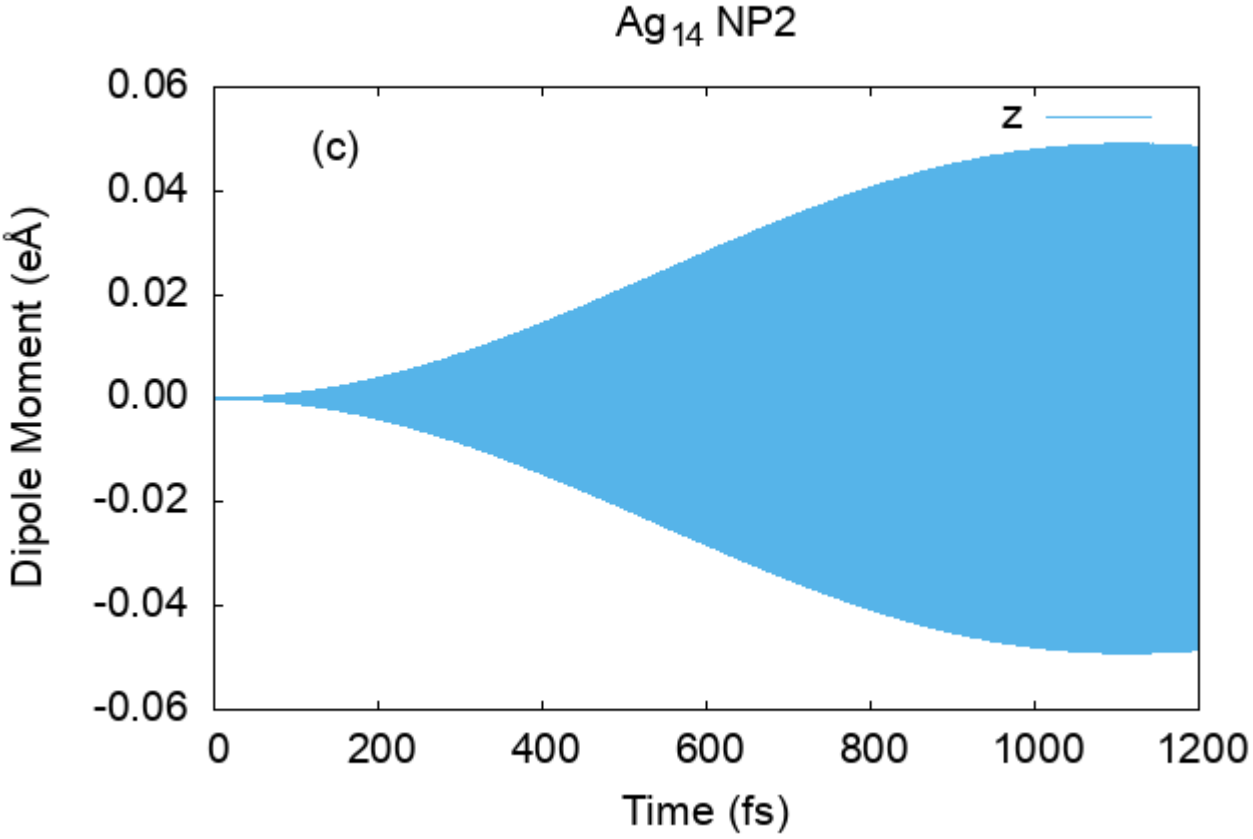
Ag 14 NP2
(c)
z
Dipole Moment (eÅ)
0.06
0.04
0.02
0.00
-0.02
-0.04
-0.06
0
200
400
600
800
1000
1200
Time (fs)

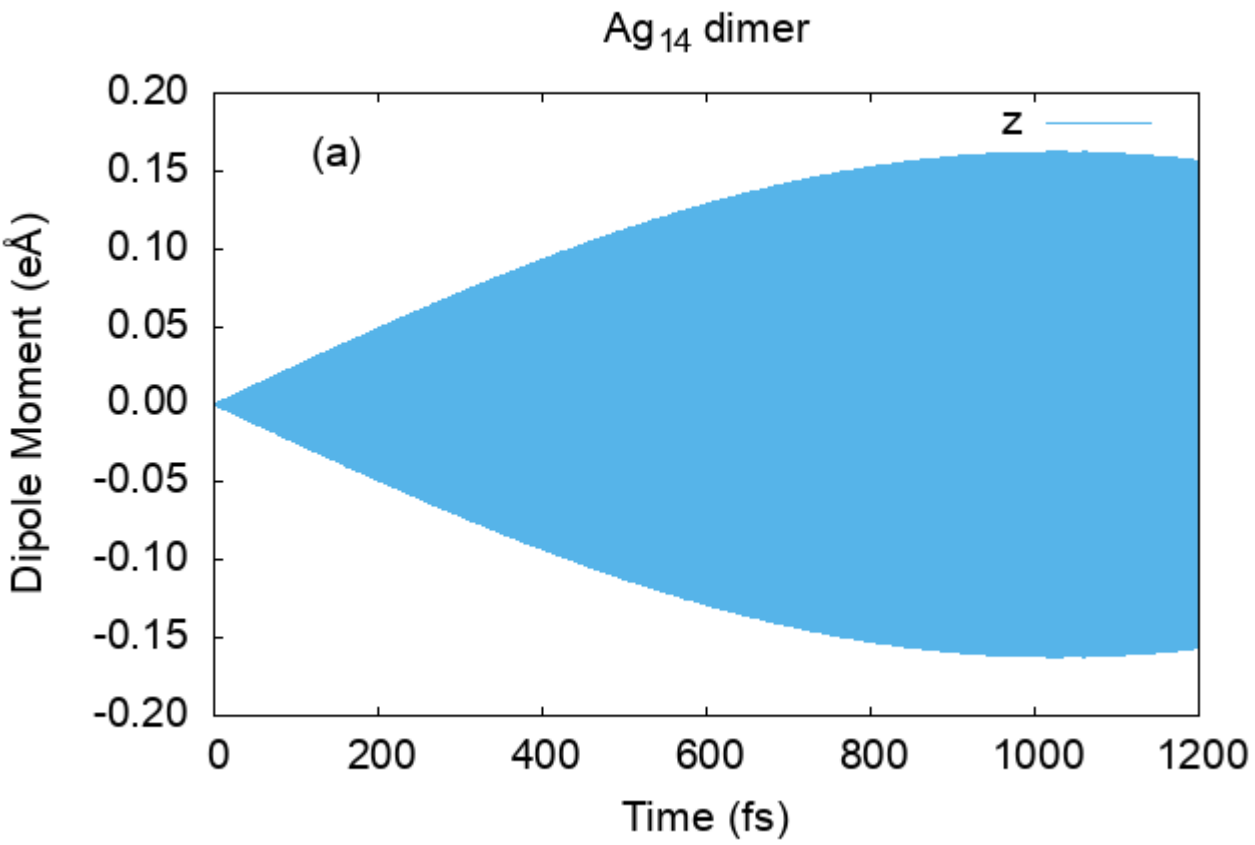
Ag 14 dimer
(a)
z
Dipole Moment (eÅ)
0.20
0.15
0.10
0.05
0.00
-0.05
-0.10
-0.15
-0.20
0
200
400
600
800
1000
1200
Time (fs)

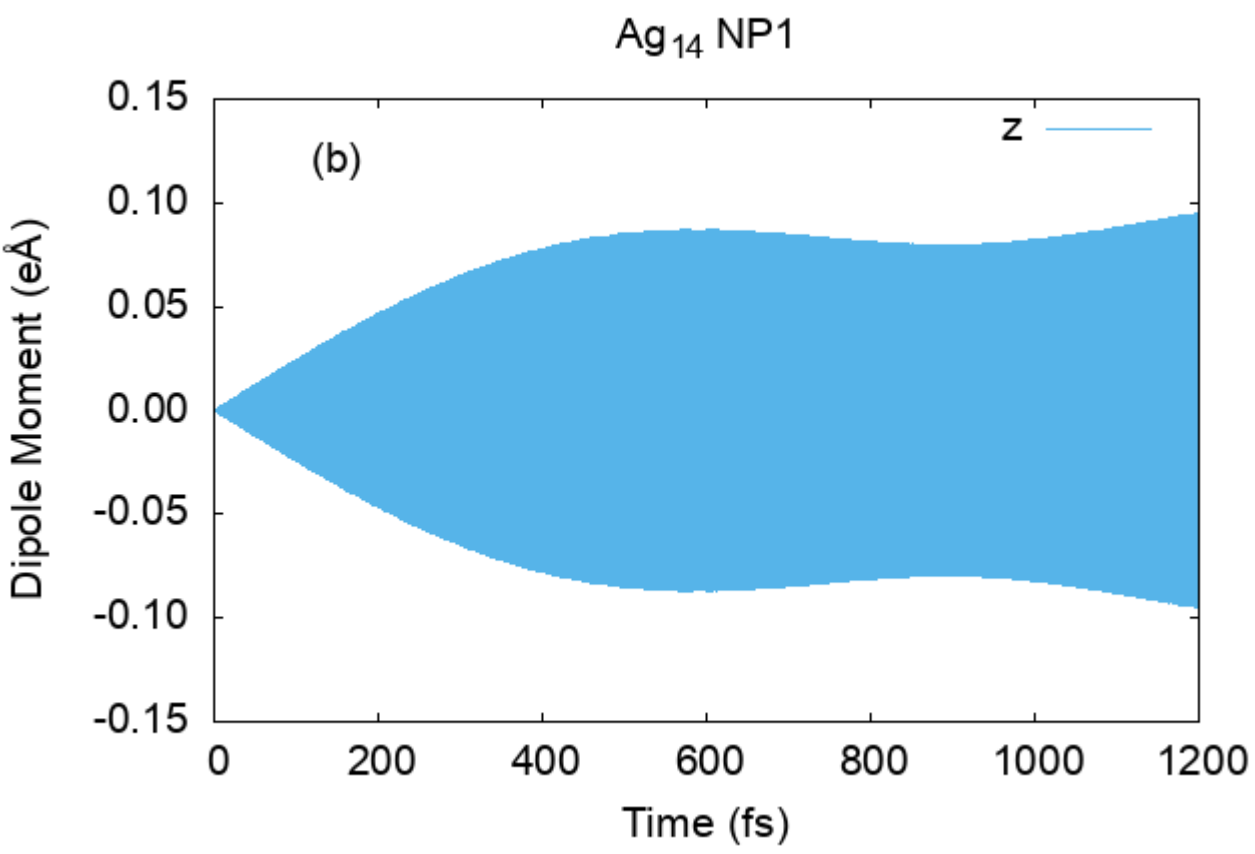
Ag 14 NP1
(b)
z
Dipole Moment (eÅ)
0.15
0.10
0.05
0.00
-0.05
-0.10
-0.15
0
200
400
600
800
1000
1200
Time (fs)

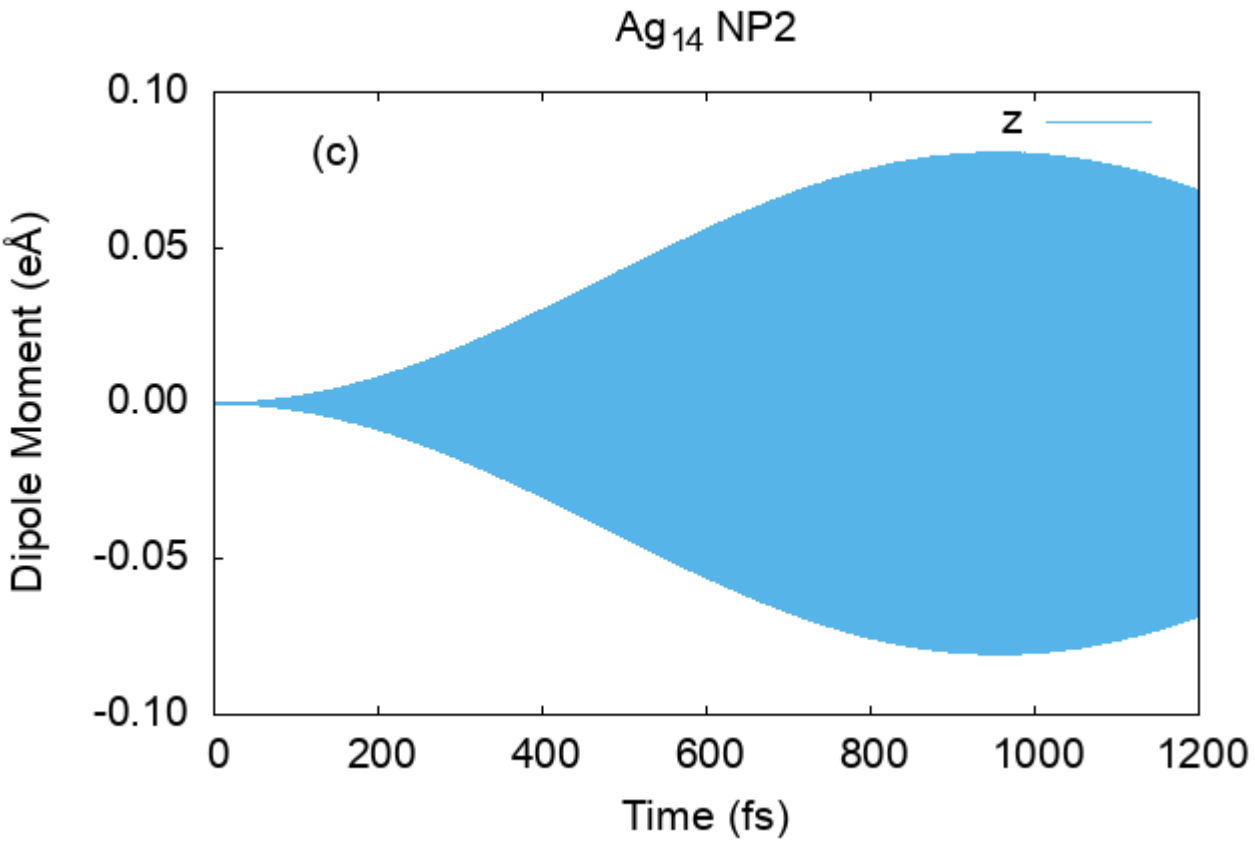
Ag 14 NP2
(c)
z
Dipole Moment (eÅ)
0.10
0.05
0.00
-0.05
-0.10
0
200
400
600
800
1000
1200
Time (fs)

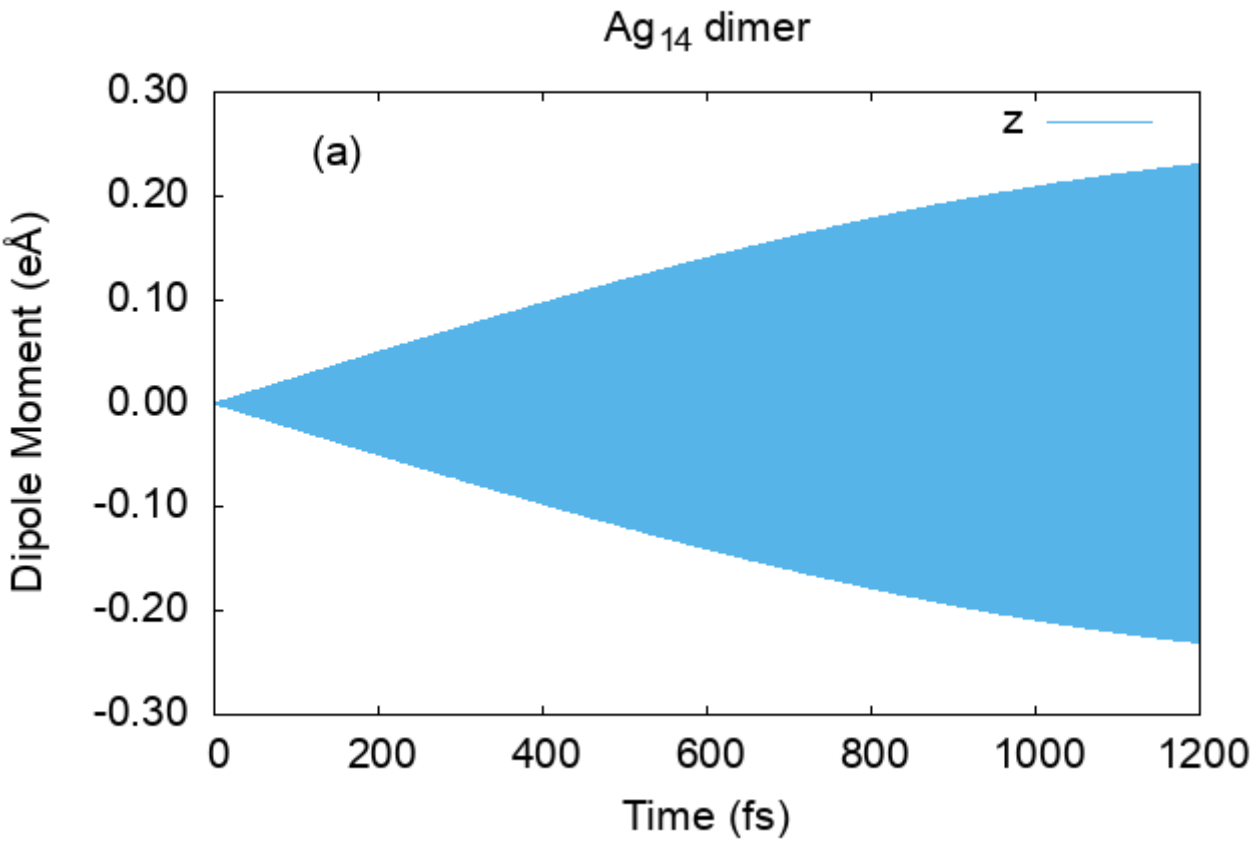
Ag 14 dimer
(a)
z
Dipole Moment (eÅ)
0.30
0.20
0.10
0.00
-0.10
-0.20
-0.30
0
200
400
600
800
1000
1200
Time (fs)

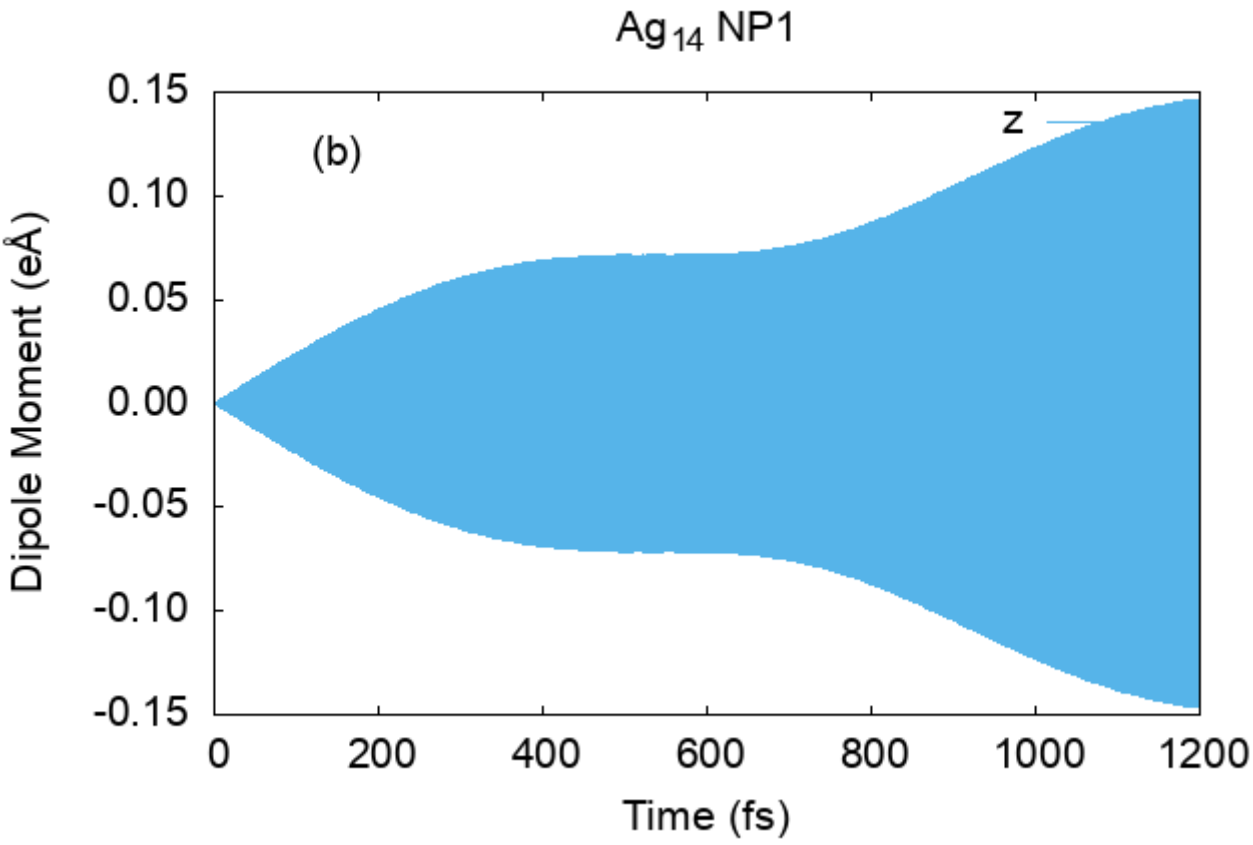
Ag 14 NP1
(b)
z
Dipole Moment (eÅ)
0.15
0.10
0.05
0.00
-0.05
-0.10
-0.15
0
200
400
600
800
1000
1200
Time (fs)

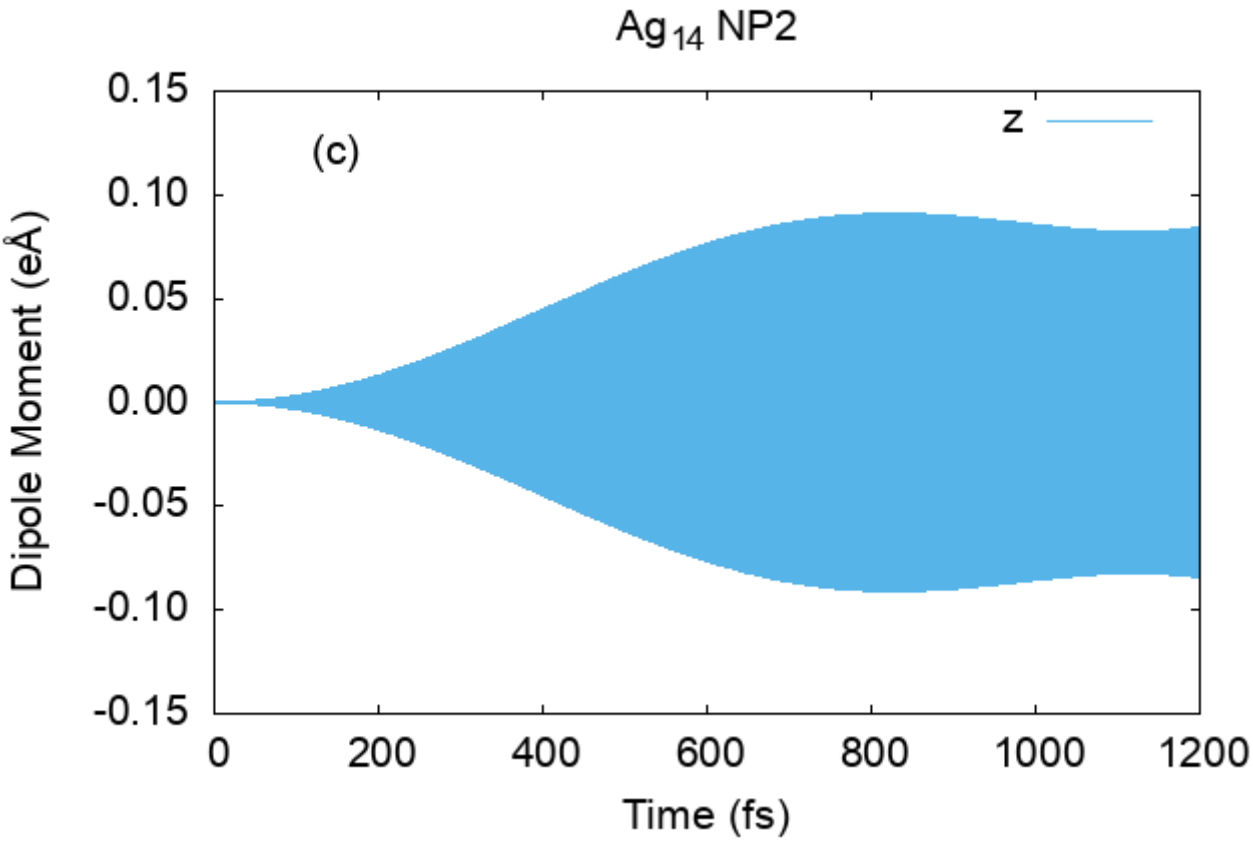
Ag 14 NP2
(c)
z
Dipole Moment (eÅ)
0.15
0.10
0.05
0.00
-0.05
-0.10
-0.15
0
200
400
600
800
1000
1200
Time (fs)

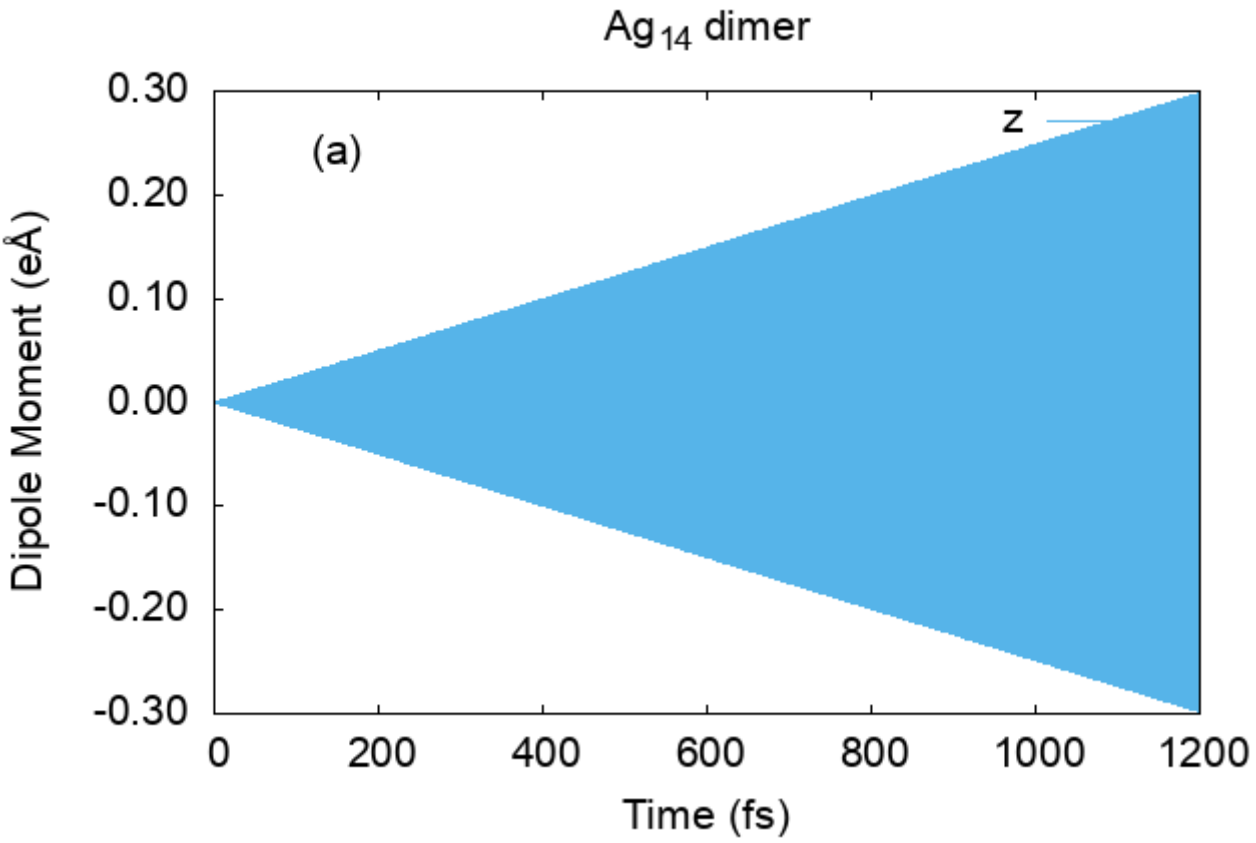
Ag 14 dimer
(a)
z
Dipole Moment (eÅ)
0.30
0.20
0.10
0.00
-0.10
-0.20
-0.30
0
200
400
600
800
1000
1200
Time (fs)

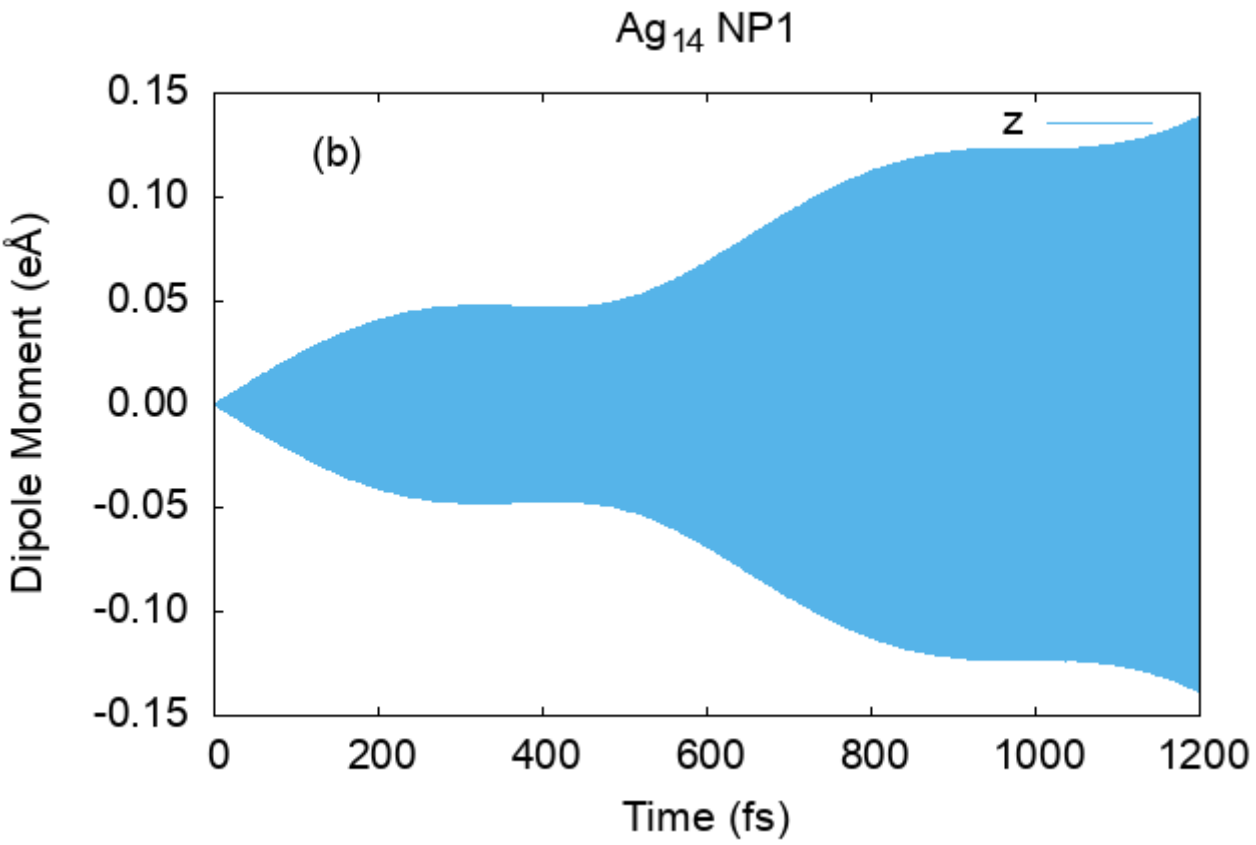
Ag 14 NP1
(b)
z
Dipole Moment (eÅ)
0.15
0.10
0.05
0.00
-0.05
-0.10
-0.15
0
200
400
600
800
1000
1200
Time (fs)

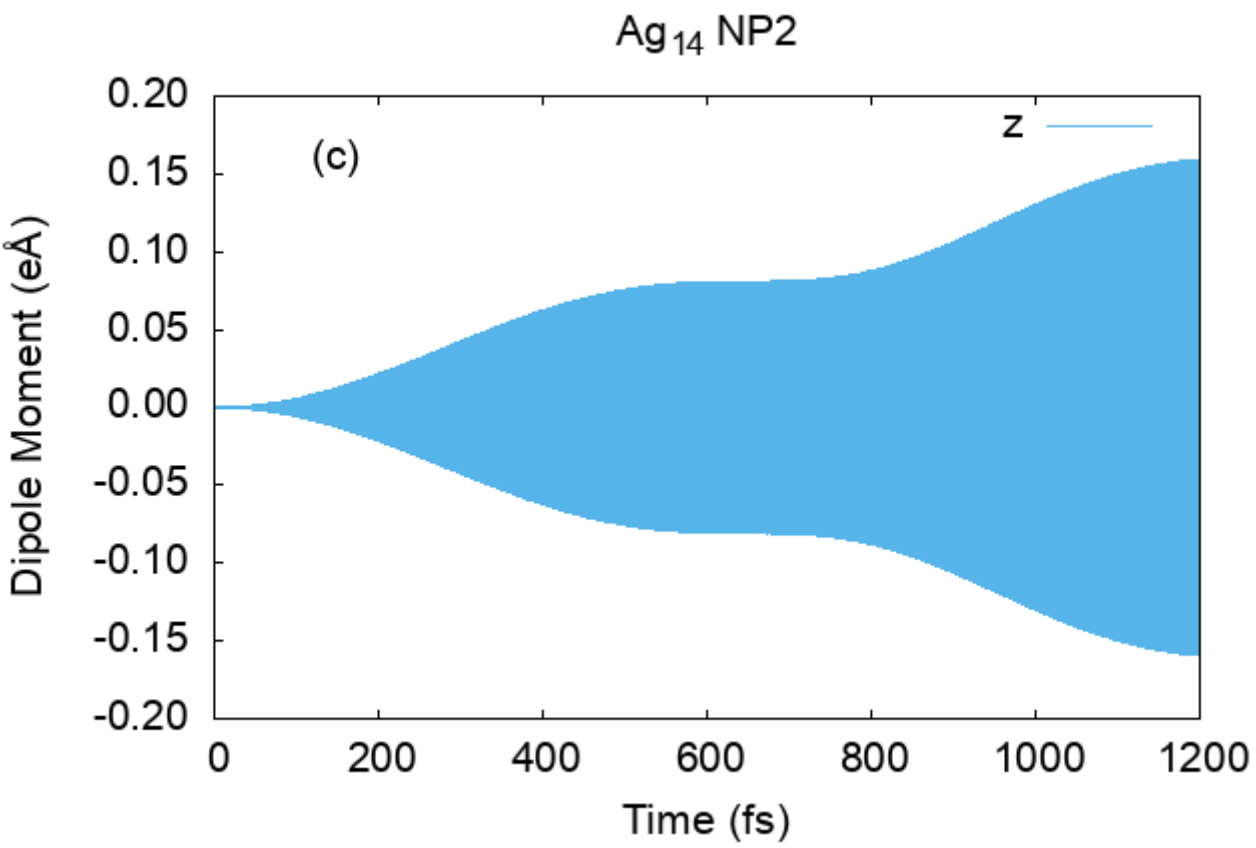
Ag 14 NP2
(c)
z
Dipole Moment (eÅ)
0.20
0.15
0.10
0.05
0.00
-0.05
-0.10
-0.15
-0.20
0
200
400
600
800
1000
1200
Time (fs)

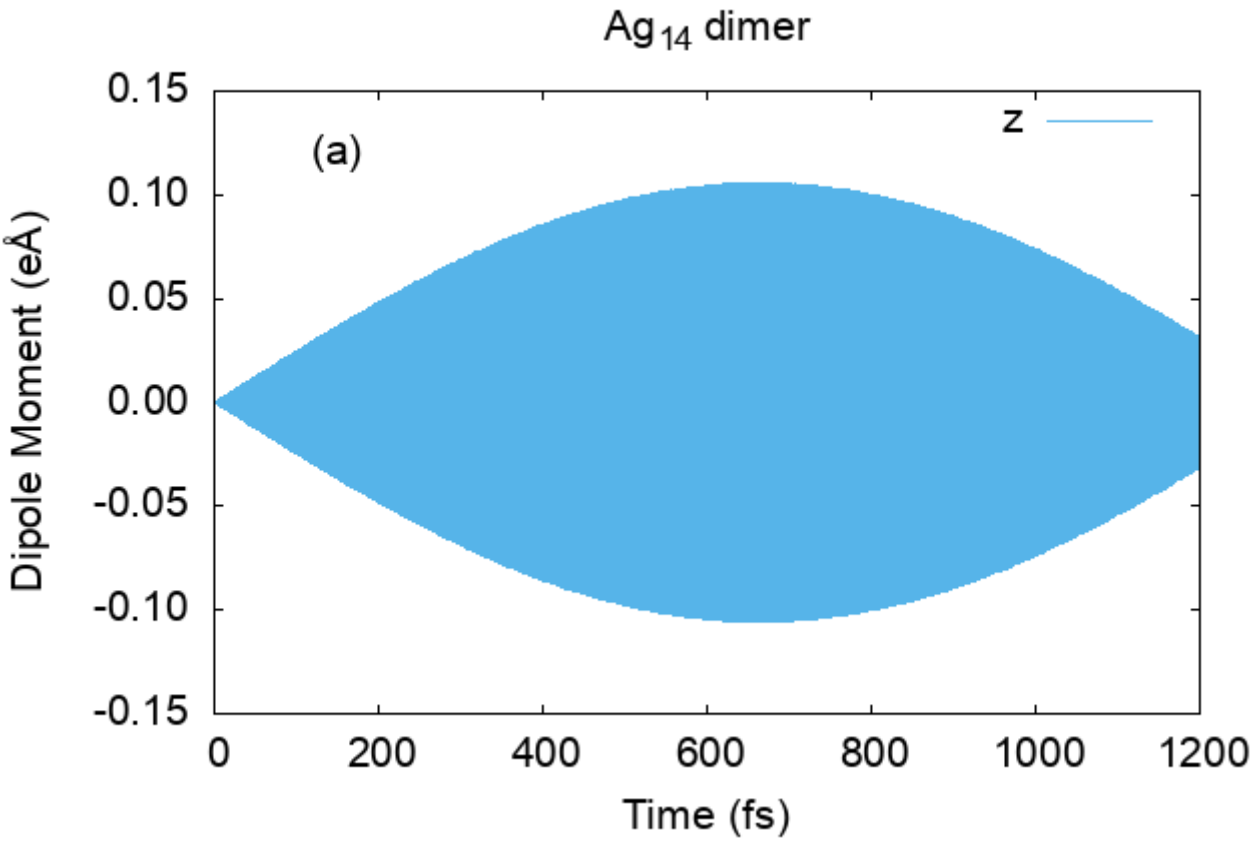
Ag14 dimer
(a)
z
Dipole Moment (eÅ)
0.15
0.10
0.05
0.00
-0.05
-0.10
-0.15
0
200
400
600
800
1000
1200
Time (fs)

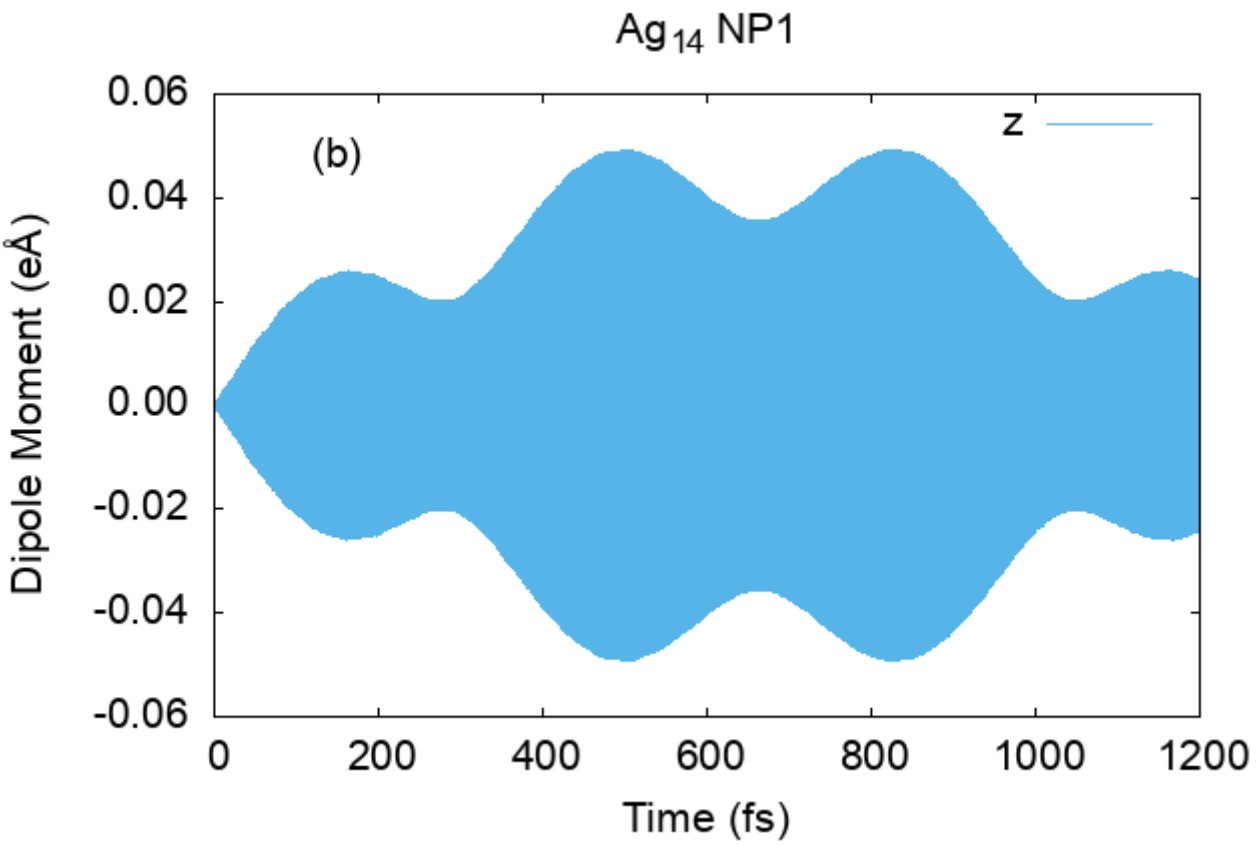
Ag14 NP1
(b)
z
Dipole Moment (eÅ)
0.06
0.04
0.02
0.00
-0.02
-0.04
-0.06
0
200
400
600
800
1000
1200
Time (fs)

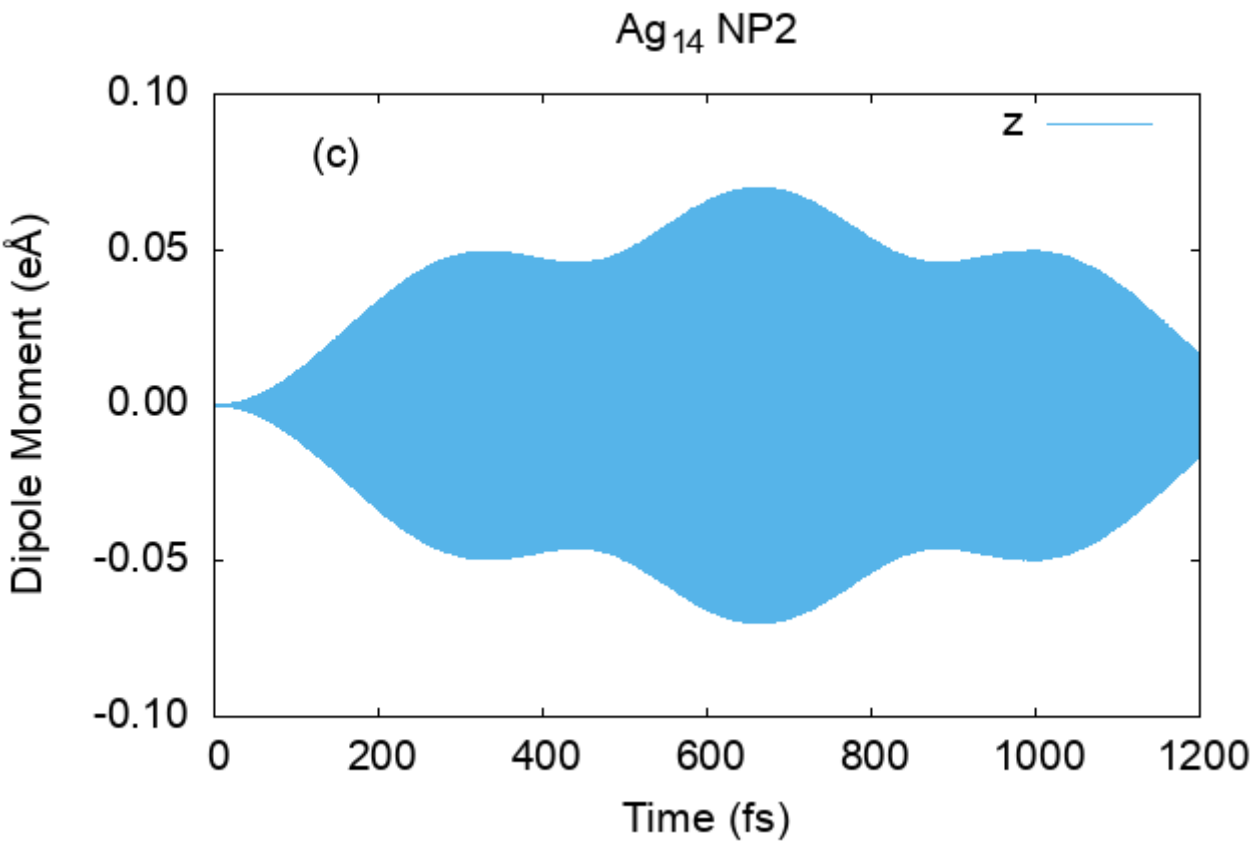
Ag14 NP2
(c)
z
Dipole Moment (eÅ)
0.10
0.05
0.00
-0.05
-0.10
0
200
400
600
800
1000
1200
Time (fs)

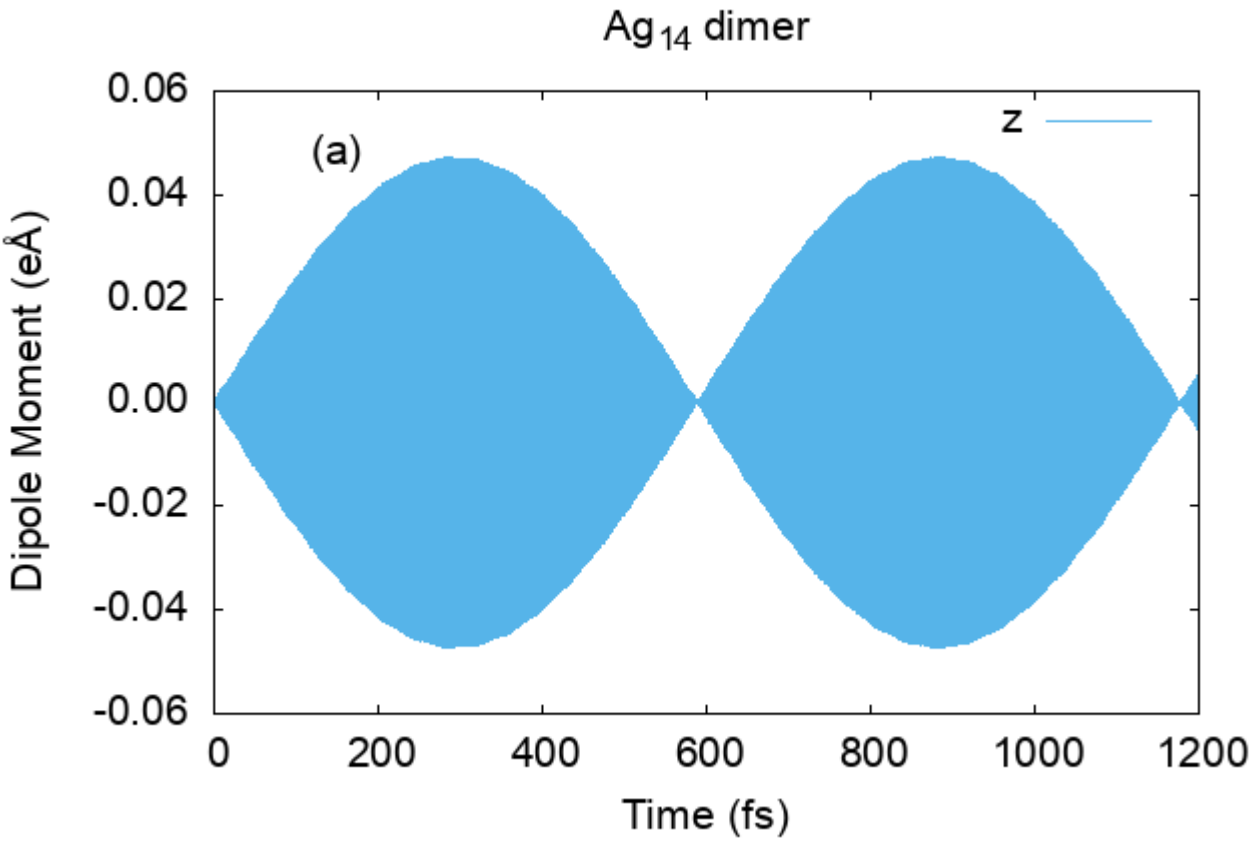
Ag14 dimer
(a)
z
Dipole Moment (eÅ)
0.06
0.04
0.02
0.00
-0.02
-0.04
-0.06
0
200
400
600
800
1000
1200
Time (fs)

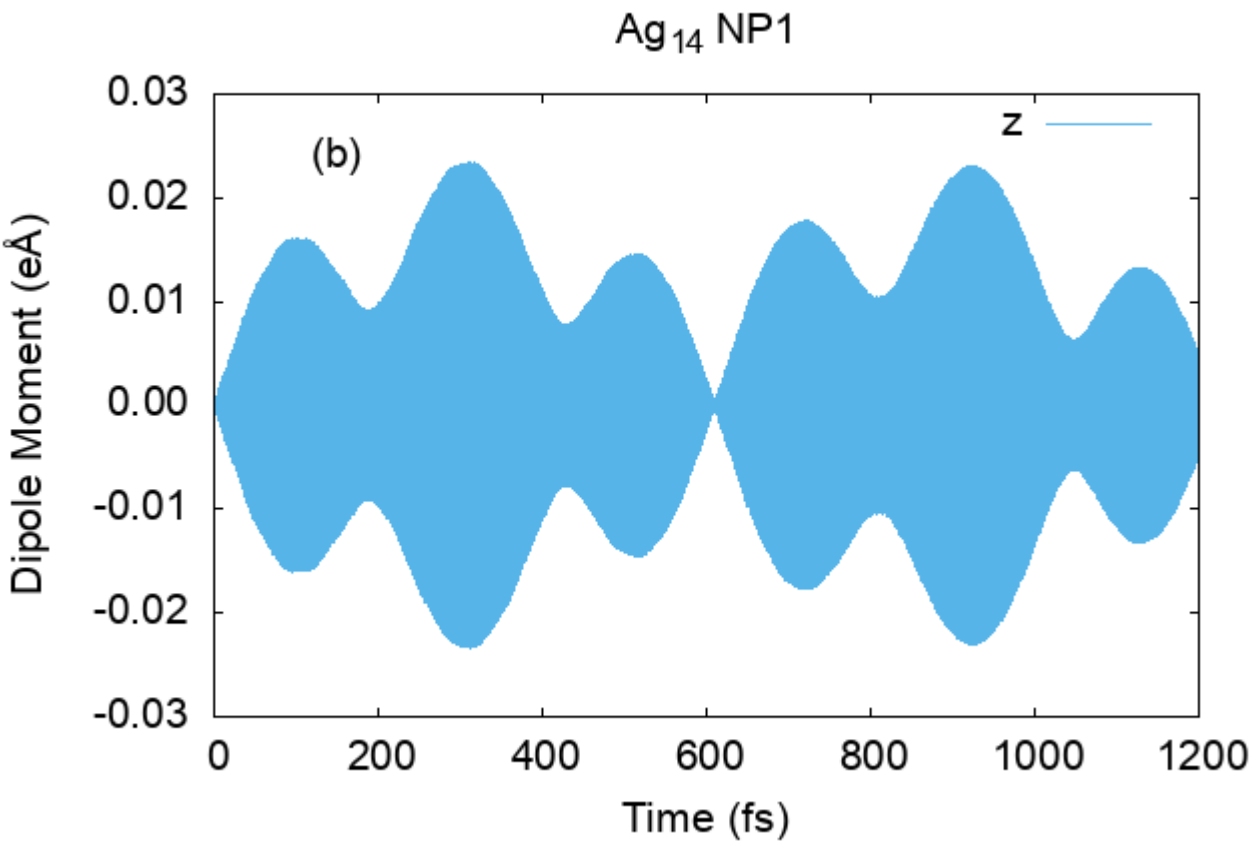
Ag14 NP1
(b)
z
Dipole Moment (eÅ)
0.03
0.02
0.01
0.00
-0.01
-0.02
-0.03
0
200
400
600
800
1000
1200
Time (fs)

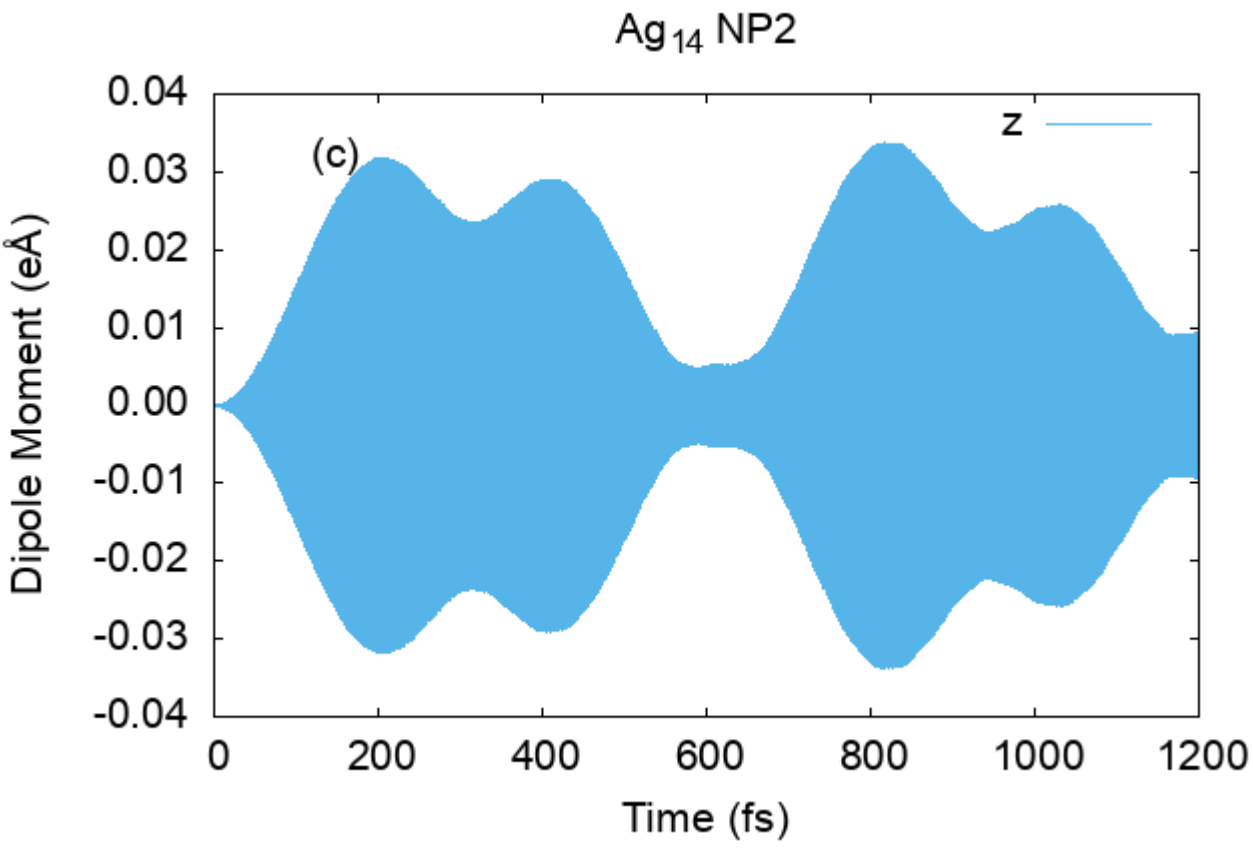
Ag14 NP2
(c)
z
Dipole Moment (eÅ)
0.04
0.03
0.02
0.01
0.00
-0.01
-0.02
-0.03
-0.04
0
200
400
600
800
1000
1200
Time (fs)

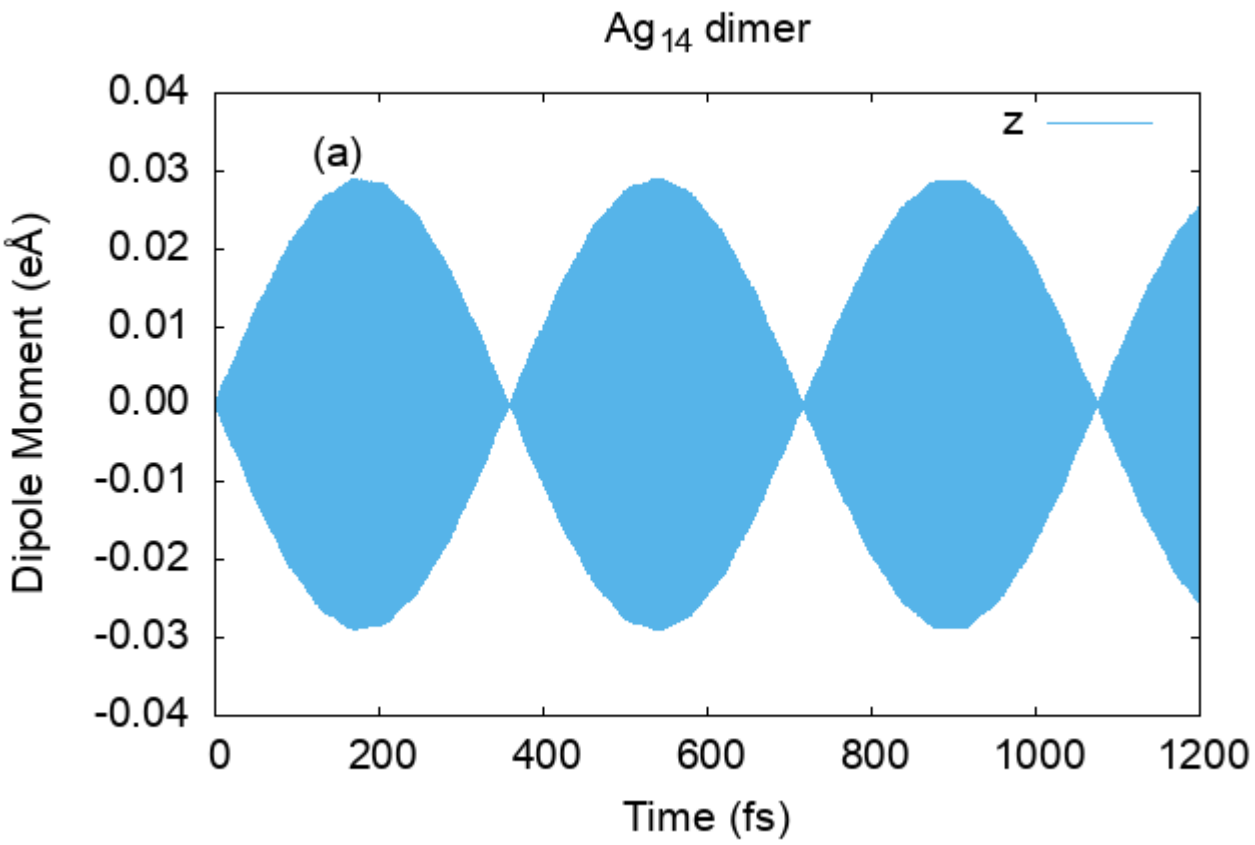
Ag 14 dimer
(a)
z
Dipole Moment (eÅ)
Time (fs)
0.04
0.03
0.02
0.01
0.00
-0.01
-0.02
-0.03
-0.04
0
200
400
600
800
1000
1200

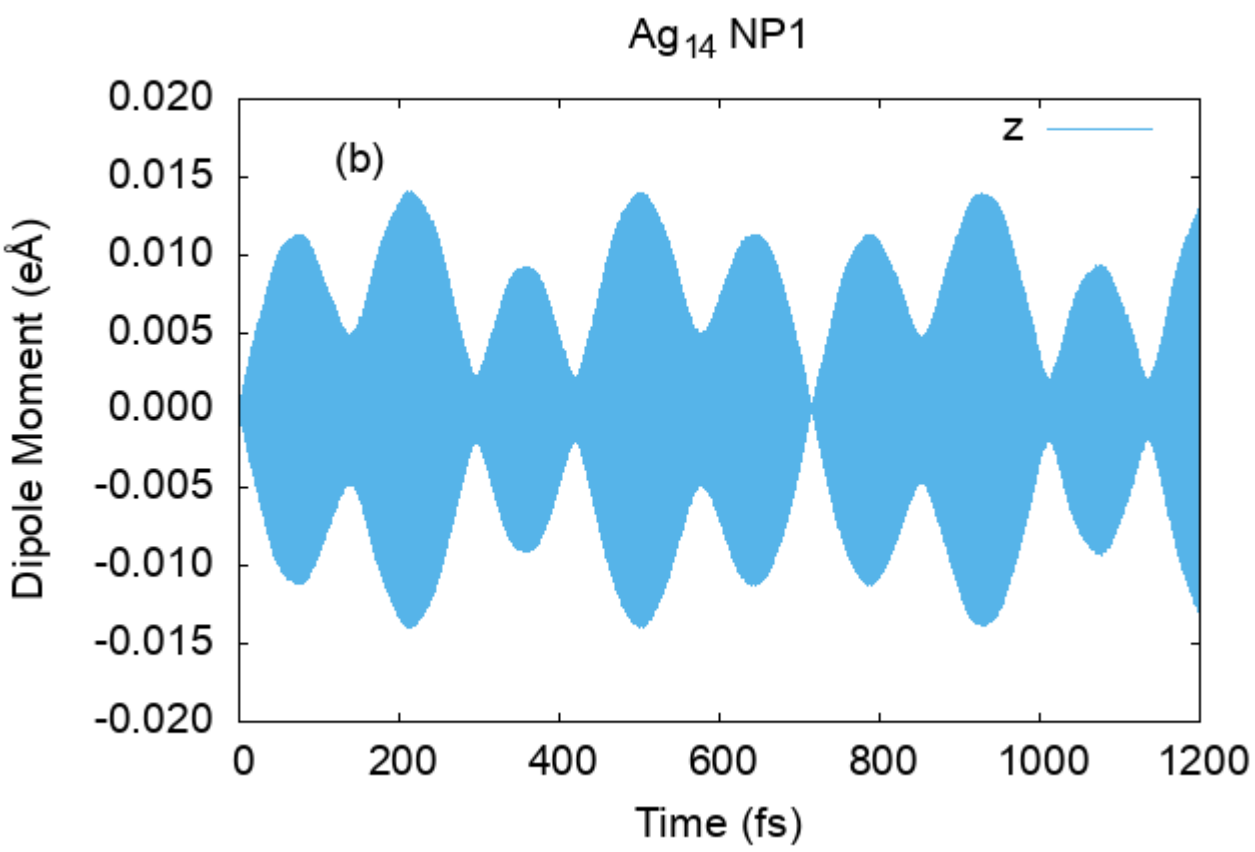
Ag 14 NP1
(b)
z
Dipole Moment (eÅ)
Time (fs)
0.020
0.015
0.010
0.005
0.000
-0.005
-0.010
-0.015
-0.020
0
200
400
600
800
1000
1200

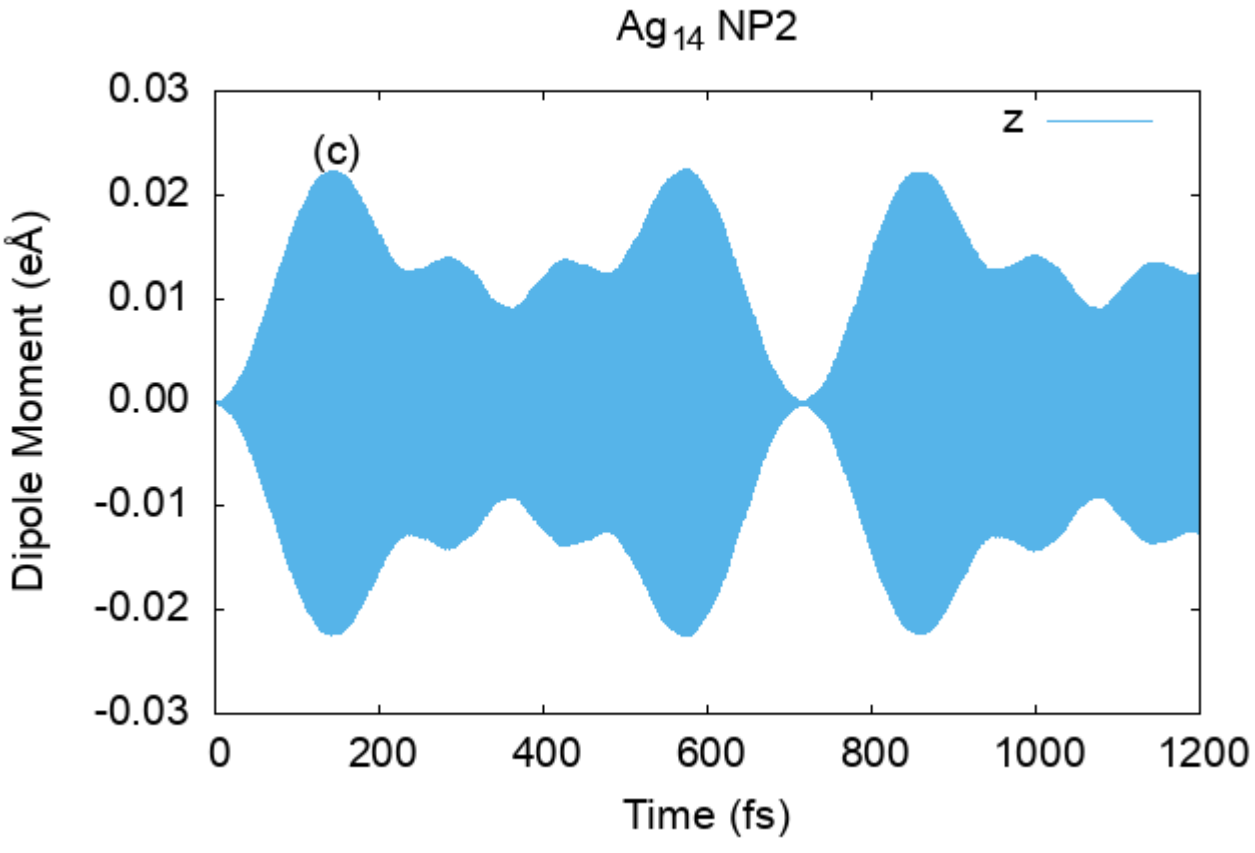
Ag 14 NP2
(c)
z
Dipole Moment (eÅ)
Time (fs)
0.03
0.02
0.01
0.00
-0.01
-0.02
-0.03
0
200
400
600
800
1000
1200

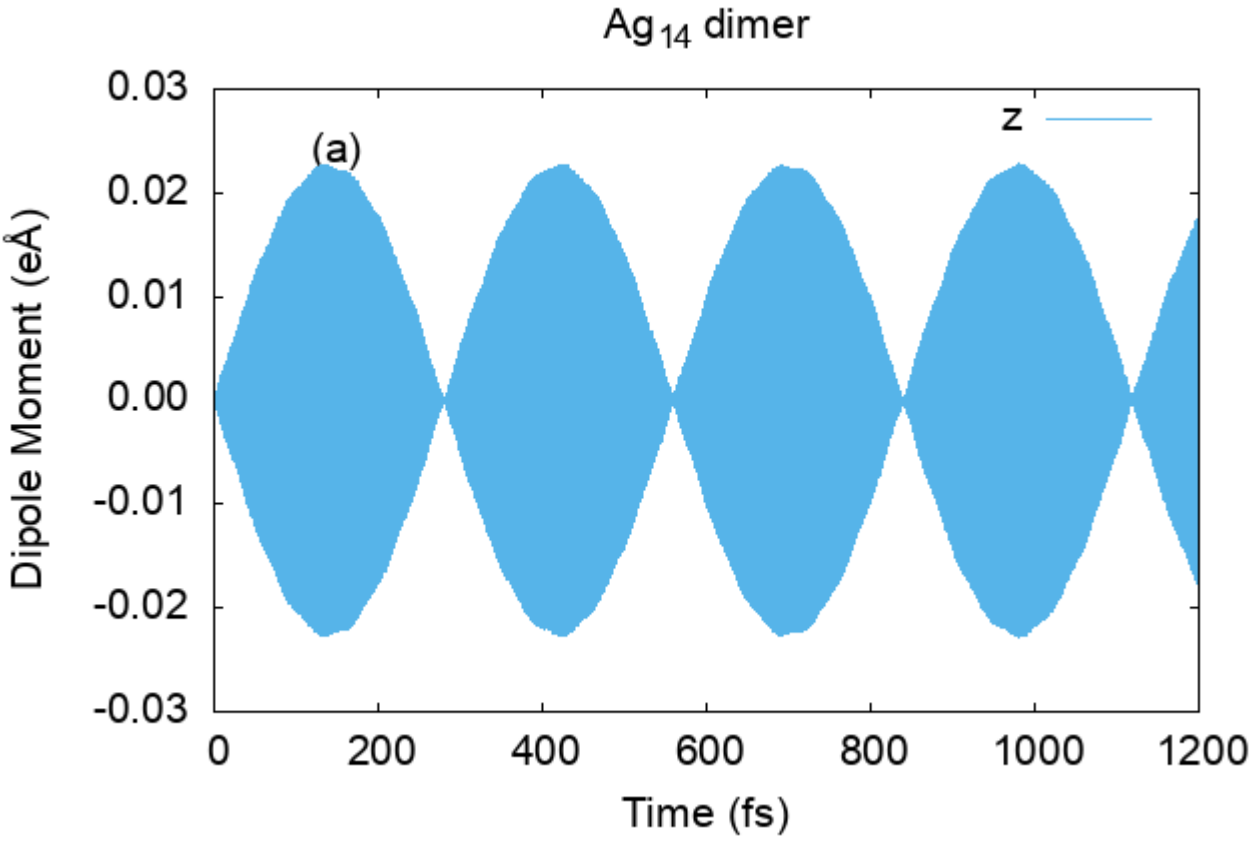
Ag 14 dimer
(a)
z
Dipole Moment (eÅ)
0.03
0.02
0.01
0.00
-0.01
-0.02
-0.03
0
200
400
600
800
1000
1200
Time (fs)

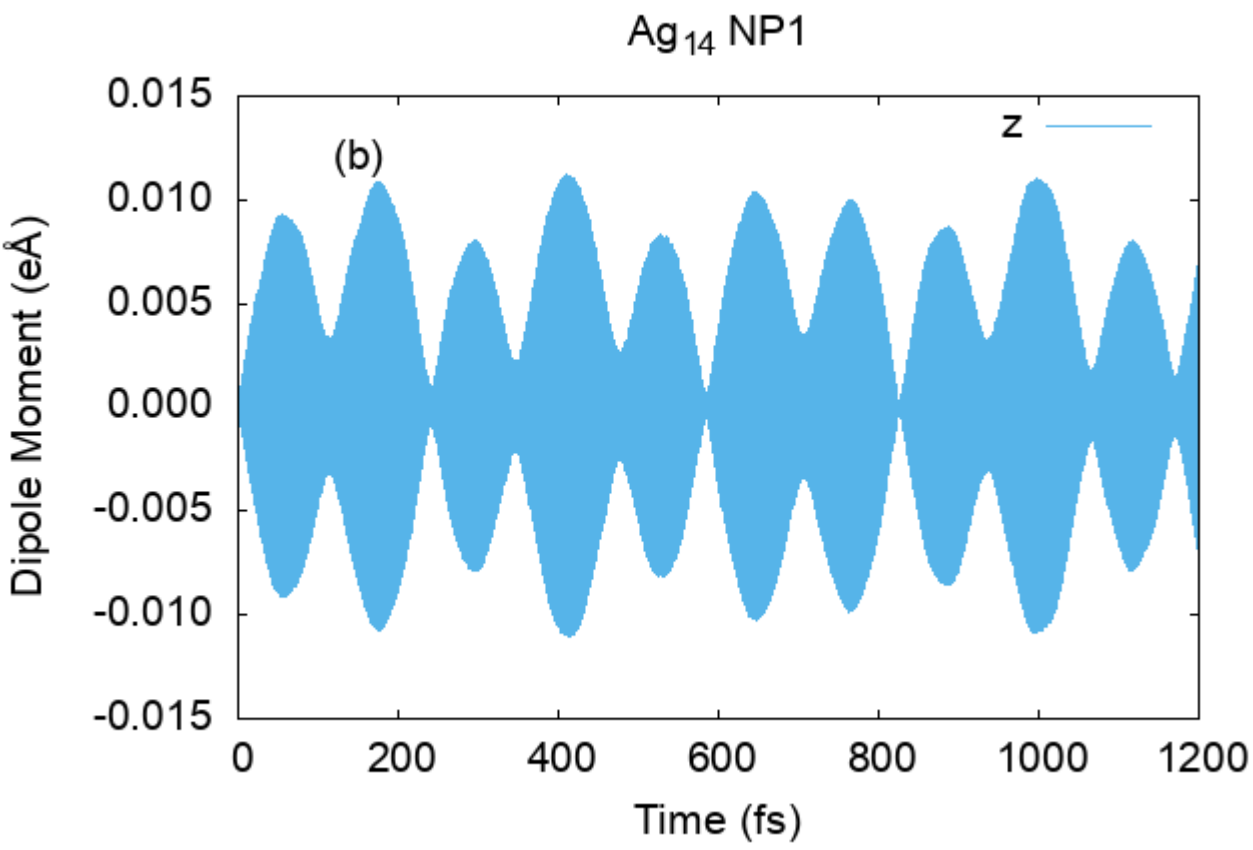
Ag 14 NP1
(b)
z
Dipole Moment (eÅ)
0.015
0.010
0.005
0.000
-0.005
-0.010
-0.015
0
200
400
600
800
1000
1200
Time (fs)

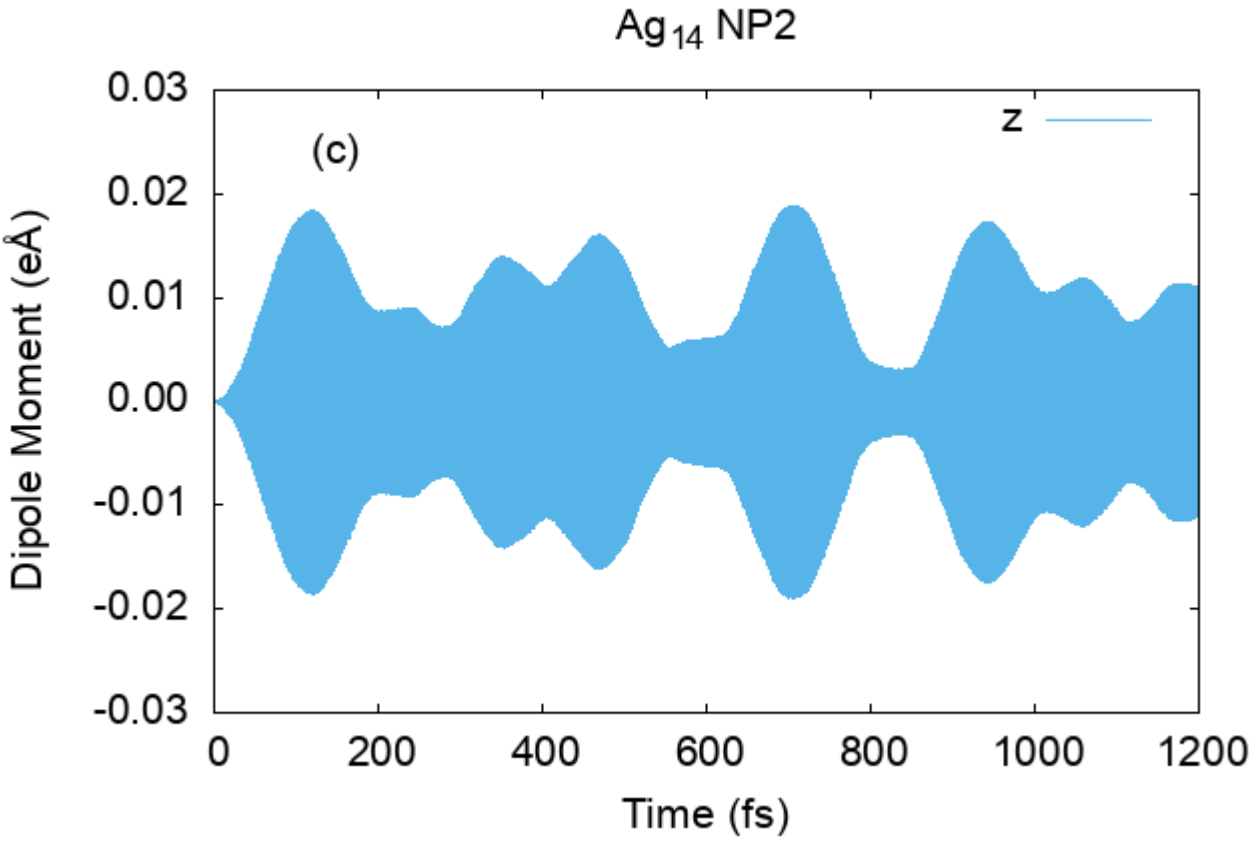
Ag 14 NP2
(c)
z
Dipole Moment (eÅ)
0.03
0.02
0.01
0.00
-0.01
-0.02
-0.03
0
200
400
600
800
1000
1200
Time (fs)

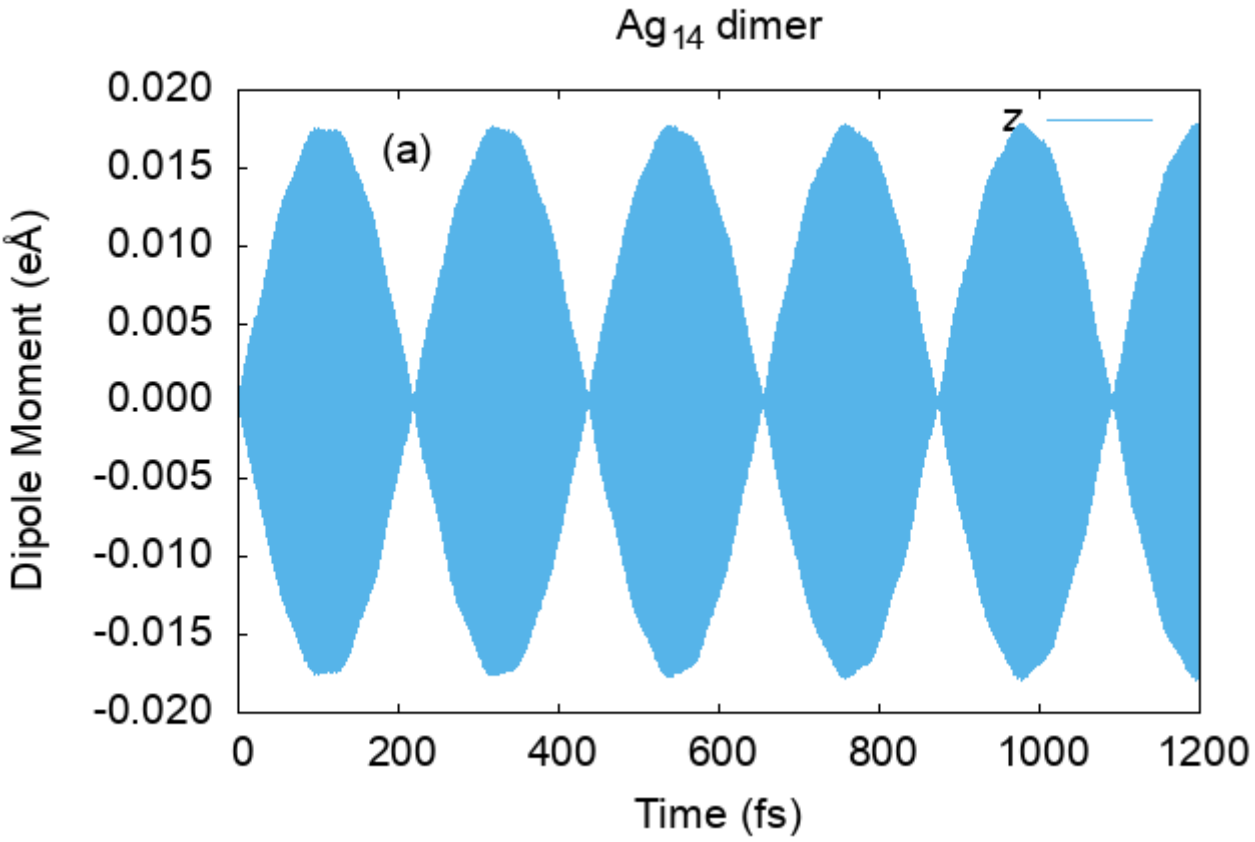
Ag 14 dimer
(a)
z
Dipole Moment (eÅ)
0.020
0.015
0.010
0.005
0.000
-0.005
-0.010
-0.015
-0.020
0
200
400
600
800
1000
1200
Time (fs)

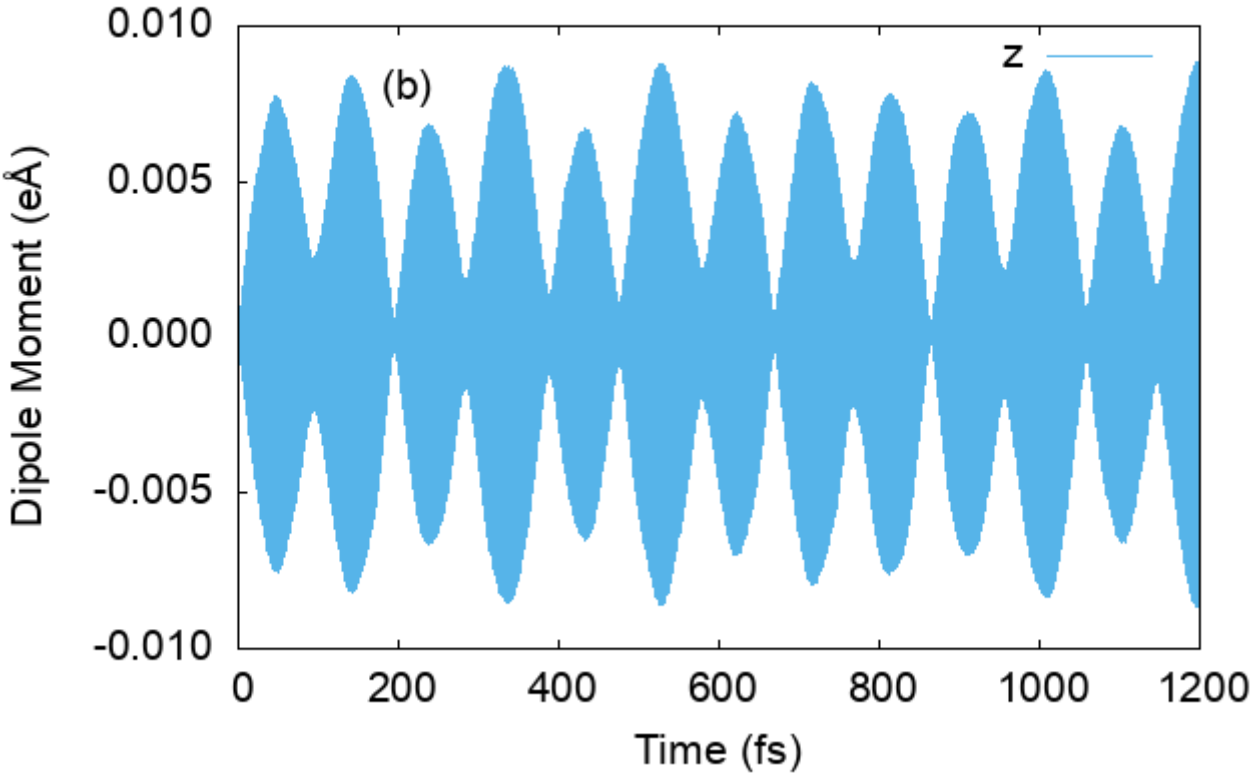
Ag 14 NP1
(b)
z
Dipole Moment (eÅ)
0.010
0.005
0.000
-0.005
-0.010
0
200
400
600
800
1000
1200
Time (fs)

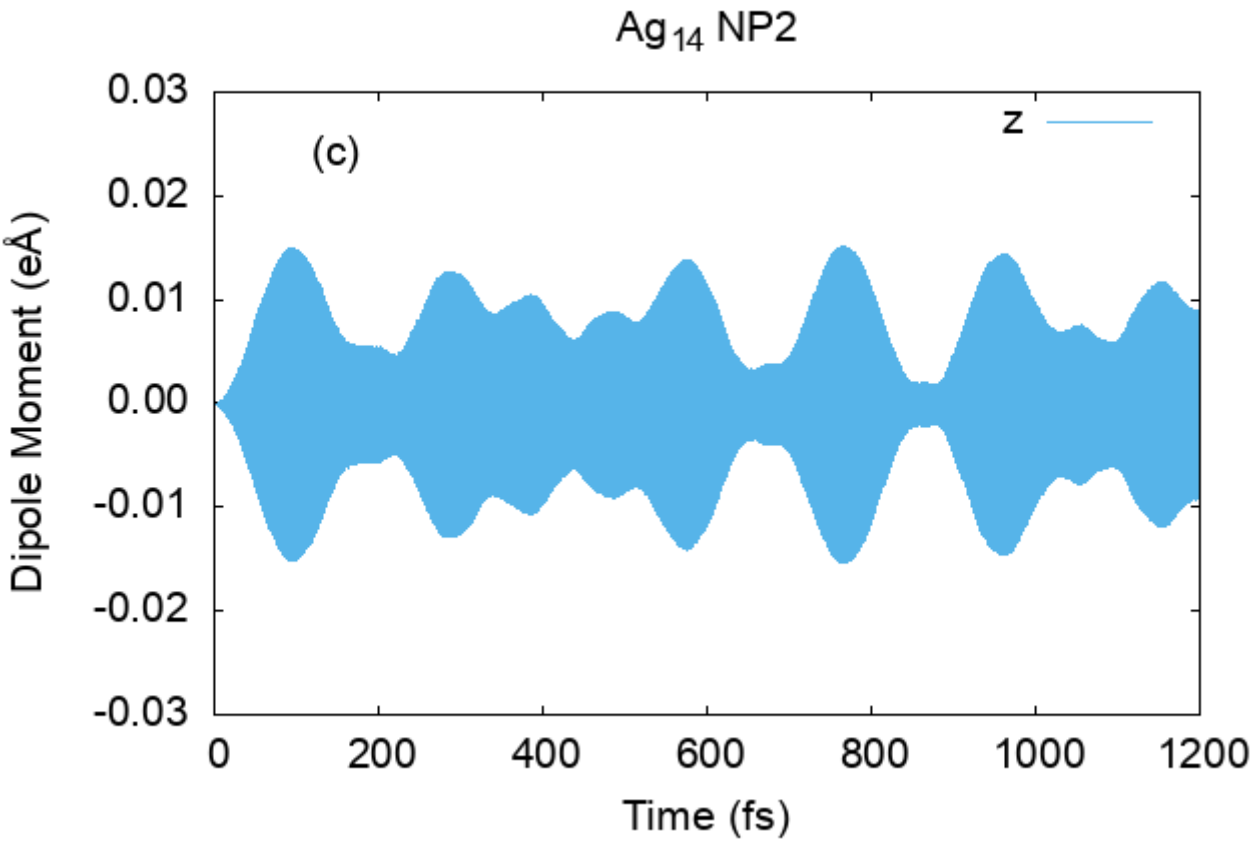
Ag 14 NP2
(c)
z
Dipole Moment (eÅ)
0.03
0.02
0.01
0.00
-0.01
-0.02
-0.03
0
200
400
600
800
1000
1200
Time (fs)